

Wiener-Hopf factorization and non-Hermitian topology for Amoeba formulation in one-dimensional multiband systems

Shin Kaneshiro* and Robert Peters

Department of Physics, Kyoto University, Kyoto 606-8502, Japan

(Dated: November 17, 2025)

The non-Hermitian skin effect (NHSE), characterized by the extensive localization of bulk modes at the boundaries, has attracted significant attention as a hallmark feature of non-Hermitian topology. This localization invalidates the conventional Bloch band theory, necessitating an analysis under open boundary conditions even in the thermodynamic limit. The Amoeba formulation addresses this challenge by computing the spectral potential rather than the spectrum itself. Based on the (strong) Szegő limit theorem and its topological generalization, this approach reduces the evaluation of the potential to an optimization problem involving the Ronkin function. However, while the generalized Szegő limit theorem is formally applicable in arbitrary dimensions, its implementation is limited to single-band systems, and its applicability to multiband systems remains unclear. In this paper, we establish the Wiener-Hopf factorization (WHF) of the non-Bloch Hamiltonian as a powerful framework, providing a unified and rigorous foundation for Amoeba analysis in multiband systems. By combining the WHF with Hermitian doubling, we first elucidate the applicability criteria for the generalized Szegő limit theorem in multiband systems. We then show that the WHF provides the natural mathematical origin for the symmetry-decomposed Ronkin function in symmetry class AII^\dagger , leading to a rigorous proof of the generalized Szegő limit theorem for these systems and opening a path toward systematic generalizations to other symmetry classes.

I. INTRODUCTION

Non-Hermitian matrices naturally arise in various kinds of systems, from classical waves to dissipative quantum systems [1–3]. The interplay of non-Hermiticity and translation symmetry fundamentally alters bulk-band topology, introducing point-gap phases without Hermitian counterparts [4, 5]. A prominent consequence is the non-Hermitian skin effect (NHSE) [6–47] where bulk eigenmodes accumulate extensively near the system boundary. This exponential localization invalidates the plane-wave expansions that underpin conventional Bloch band theory. As a result, the Fourier-based approach under periodic boundary conditions (PBC) no longer approximates systems under open boundary conditions (OBC), often necessitating a direct analysis of the OBC Hamiltonian. However, a real-space treatment can obscure the underlying bulk topology and is susceptible to numerical instabilities.

For one-dimensional systems, the non-Bloch band theory [7, 9], provides a comprehensive framework for describing OBC spectral, topological, and dynamical properties [48–73]. In this theory, the eigenmodes are expanded using exponentially modulated plane waves, known as non-Bloch states, whose complex wavenumbers trace out the generalized Brillouin zone (GBZ) [7, 9]. Extending this framework to higher dimensions, however, remains a significant challenge, since the localization behavior can no longer be encoded by a single complex momentum. As a result, several distinct formulations have been proposed [74–81].

The Amoeba formulation [82–87] addresses this challenge by focusing on the spectral potential, a thermodynamic-limit quantity derived from the characteristic polynomial under OBC. Through the (strong) Szegő limit theorem [88–90] and its topological generalization [83], this OBC spectral potential can be related to a modulated PBC spectral potential, allowing the computation to be performed in momentum space. These results imply that the OBC spectral potential can be obtained by optimizing the Ronkin function, whose argument directly controls the inverse localization length of non-Bloch waves.

While the generalized Szegő limit theorem is, in principle, applicable in arbitrary spatial dimensions, the current Amoeba formalism based on this theorem is limited to single-band systems. In multiband settings, the Ronkin function mixes contributions across bands; when degenerate states with different localization lengths occur, these contributions compete during the optimization of the Ronkin function, causing the standard Amoeba formulation to fail even in one dimension. This breakdown is unavoidable in the presence of symmetry-protected degeneracies, such as for a transpose-type time-reversal symmetry (TRS^\dagger), where Kramers pairs localize on opposite edges.

In multiband settings, one might hope to resolve the failure of the Amoeba formulation by decomposing the Ronkin function into bandwise contributions. However, a straightforward mathematical decomposition is generally not feasible: the mathematical properties of the Ronkin function are typically not preserved under bandwise separation. In the presence of TRS^\dagger , we previously demonstrated that a symmetry-guided, phenomenological decomposition consistent with non-Bloch band theory [48] can nevertheless be constructed, leading to the

* kaneshiro.shin.88a@st.kyoto-u.ac.jp

symmetry-decomposed Ronkin functions that separate the contributions of Kramers pairs while retaining the required structure [91]. Nevertheless, its relation to the generalized Szegő limit theorem remained unclear, and extensions beyond TRS^\dagger , particularly to class A multi-band systems without protecting symmetries, were still lacking.

Originally, the Szegő limit theorem was formulated using the Wiener-Hopf factorization (WHF) for topologically trivial Hamiltonians [89, 90]. Recently, Ref. [92] demonstrated that the WHF itself offers a direct topological interpretation for Hermitian Hamiltonians: the WHF partial indices count the number of edge modes and thereby establish the bulk-boundary correspondence. This intimate connection between WHF and topology is central to the generalization of the original theorem to topologically nontrivial Hermitian Hamiltonians, a result known as the Modified Szegő limit theorem [93].

Inspired by these developments, we apply the WHF in this paper to non-Hermitian systems combined with Hermitian doubling [4, 5]. We demonstrate that the WHF of a non-Hermitian non-Bloch Hamiltonian faithfully captures its topological properties. Moreover, this framework allows us to identify the WHF partial indices as the exact criteria determining when the generalized Szegő limit theorem remains valid in multiband systems. By reinterpreting the generalized Szegő limit theorem as a corollary of the modified Szegő theorem, we derive the necessary correction terms to the optimization formalism. Finally, this approach reveals the mathematical origin of the symmetry-decomposed Ronkin functions and provides a direct proof of the generalized Szegő limit theorem for class AII^\dagger systems.

The remainder of this paper is organized as follows. In Sec. II, we introduce our notation and summarize the Amoeba formulation in one-dimensional class A and AII^\dagger systems. Sec. III reviews the Wiener-Hopf factorization (WHF) for Hermitian Hamiltonians and relates it to band topology via partial indices. Next, we generalize this framework to non-Hermitian Hamiltonians via Hermitian doubling. Section IV develops the connection between WHF and the Szegő limit theorem in multiband systems, including the modified Szegő theorem, and clarifies the precise criteria under which the OBC and PBC spectral potentials coincide. Building on this groundwork, Sec. V presents the central theoretical results of this paper. We reformulate the generalized Szegő limit theorem as a corollary of the modified Szegő theorem via Hermitian doubling, derive the necessary correction terms for the multiband Amoeba formulation, and provide a rigorous mathematical foundation for the symmetry-decomposed Ronkin functions in class AII^\dagger systems. In Sec. VI, we validate our theoretical framework through numerical studies on representative models. Section VII concludes with a summary and outlook. Finally, Appendix A analyzes the fragility of the $\kappa = 2$ phase discussed in Sec. VI, showing that it is unprotected by TRS^\dagger and disappears under small

TRS^\dagger -preserving perturbations.

II. AMOEBA FORMULATION IN ONE-DIMENSIONAL SYSTEMS

This section introduces the notation and provides a brief review of the Amoeba formulation in classes A [83] and AII^\dagger [91] systems.

A. Notation

We consider an M -band Bloch Hamiltonian of finite hopping range,

$$h(e^{ik}) = \sum_{j=-p}^q h_j e^{ikj}, \quad (1)$$

where p and q denote the maximal hopping range to the left and right, respectively. Each h_j is an $M \times M$ matrix specifying the hopping amplitudes between orbitals separated by j sites.

Substituting $\beta = e^{ik}$, $h(\beta)$ is a matrix-valued Laurent polynomial

$$h(\beta) = \sum_{j=-p}^q h_j \beta^j, \quad (2)$$

which we refer to as the non-Bloch Hamiltonian.

From the Fourier coefficients $\{h_j\}$, we construct the OBC Hamiltonian on a one-dimensional lattice with N sites,

$$[H_N]_{x,y} = h_{x-y} \quad (1 \leq x, y \leq N), \quad (3)$$

with the convention $h_l = 0$ for $l \notin [-p, q]$. Equivalently, the inverse Fourier transform of h generates an $N \times N$ Toeplitz matrix $\mathcal{T}_N[h]$

$$[H_N]_{x,y} = \mathcal{T}_N[h]_{x,y} = \int_0^{2\pi} \frac{dk}{2\pi} h(e^{ik}) e^{-ik(x-y)}. \quad (4)$$

We define Hermitian conjugate, transpose, and complex conjugation on matrix-valued polynomials of $h(\beta)$ so that they commute with \mathcal{T}_N :

$$\begin{aligned} \mathcal{T}_N[h]^\dagger &= \mathcal{T}_N[h^\dagger], & \mathcal{T}_N[h]^\top &= \mathcal{T}_N[h^\top], \\ \mathcal{T}_N[h]^* &= \mathcal{T}_N[h^*], \end{aligned} \quad (5)$$

where

$$\begin{aligned} h^\dagger(\beta) &= \sum_j h_j^\dagger \beta^{-j}, & h^\top(\beta) &= \sum_j h_j^\top \beta^{-j}, \\ h^*(\beta) &= \sum_j h_j^* \beta^j. \end{aligned} \quad (6)$$

We stress that Hermitian conjugation and transpose reverse the Laurent powers ($\beta^j \mapsto \beta^{-j}$), whereas complex conjugation acts only on the coefficients and leaves the powers β^j unchanged.

B. Amoeba formulation for class A

We now focus on one-dimensional single-band systems ($M = 1$) in class A, i.e., systems without symmetry constraints. The Amoeba formulation determines the OBC spectrum through its DOS defined over the complex energy plane. The DOS is defined using Dirac's delta functions as

$$\rho(E) = \lim_{N \rightarrow \infty} \frac{1}{N} \text{Tr} \delta(E - H_N). \quad (7)$$

Viewing $\rho(E)$ as a two-dimensional charge density, the spectral potential $\phi(E)$ is defined by the Poisson equation

$$\rho(E) = \frac{1}{2\pi} \Delta \phi(E), \quad (8)$$

where $\Delta = \partial^2/\partial(\text{Re } E)^2 + \partial^2/\partial(\text{Im } E)^2$. We can easily find that $\phi(E)$ takes the form

$$\phi(E) = \lim_{N \rightarrow \infty} \frac{1}{N} \ln |\det \mathcal{T}_N[E - h]|. \quad (9)$$

Let $\sigma(\beta) = E - h(\beta)$ denote the non-Hermitian symbol of the system. We assume that $\sigma(\beta)$ is invertible for all β with absolute value 1 and topologically trivial, i.e., the winding number

$$W[\sigma] = \int_0^{2\pi} \frac{dk}{2\pi i} \partial_k \ln \det \sigma(e^{ik}), \quad (10)$$

is well-defined and vanishes. Then $\mathcal{T}_N[\sigma]$ is invertible, and Szegő limit theorem yields [88],

$$\lim_{N \rightarrow \infty} \frac{1}{N} \ln \det \mathcal{T}_N[\sigma] = \int_0^{2\pi} \frac{dk}{2\pi} \ln \det \sigma(e^{ik}). \quad (11)$$

This theorem states that the OBC and PBC spectral potentials coincide for such E .

For an arbitrary (possibly topologically nontrivial) energy E , the diagonal similarity transformation

$$D_N^{(\mu)} \mathcal{T}_N[\sigma] [D_N^{(\mu)}]^{-1} = \mathcal{T}_N[\sigma_\mu], \quad (12)$$

where $[D_N^{(\mu)}]_{x,y} = \delta_{x,y} e^{\mu x}$ and $\sigma_\mu(e^{ik}) = \sigma(e^{\mu+ik})$, maps the Toeplitz matrix $\mathcal{T}_N[\sigma]$ to one defined by the analytically continued symbol σ_μ . Since the determinant is invariant under similarity transformations, $\det \mathcal{T}_N[\sigma] = \det \mathcal{T}_N[\sigma_\mu]$. Hence, if there exists a μ such that $W[\sigma_\mu] = 0$, Szegő limit theorem Eq. (11) can be applied for σ_μ :

$$\lim_{N \rightarrow \infty} \frac{1}{N} \ln \det \mathcal{T}_N[\sigma] = \int_0^{2\pi} \frac{dk}{2\pi} \ln \det \sigma_\mu(e^{ik}). \quad (13)$$

This discussion is equivalent to the optimization problem

$$\phi(E) = \min_{\mu} R_\sigma(\mu), \quad (14)$$

where R_σ is the Ronkin function defined as

$$R_\sigma(\mu) = \int_0^{2\pi} \frac{dk}{2\pi} \ln |\det \sigma_\mu(e^{ik})|, \quad (15)$$

and its derivative with respect to μ directly yields the winding number, $W[\sigma_\mu]$.

The Ronkin function can be rewritten in a compact form using the factorization

$$\det \sigma(\beta) = C_E \beta^{-p} \prod_{j=1}^{p+q} [\beta - \beta_j(E)], \quad (16)$$

where C_E is a β -independent coefficient and the β -roots are ordered by increasing modulus. With this factorization, the Ronkin function is written as

$$R_\sigma(\mu) = \ln |C_E| - p\mu + \sum_{j=1}^{p+q} \max(\mu, \mu_j), \quad (17)$$

where $\mu_j = \ln |\beta_j|$. The second and third terms are the contributions from the pole and roots of $\det \sigma$, respectively.

Using this compact expression, one finds that $R_\sigma(\mu)$ attains its minimum within the interval $[\mu_p, \mu_{p+1}]$, which precisely corresponds to the GBZ condition [7, 9]. In this region, the transformed symbol σ_μ is topologically trivial, corresponding to a vanishing winding number $W[\sigma_\mu] = 0$. For energies on the OBC spectrum, this interval collapses to a single value of μ , whose magnitude gives the inverse localization length of the corresponding eigenstate. Minimization over μ gives the compact expression of the potential

$$\phi(E) = \min_{\mu} R_\sigma(\mu) = \ln |C_E| + \sum_{j=p+1}^{p+q} \mu_j. \quad (18)$$

C. Amoeba formulation for class AII[†]

The Amoeba formulation requires modification in the presence of symmetry-protected degeneracies. We recently addressed this issue in Ref. [91]; Below, we summarize the relevant results for later use.

In this section, we consider one-dimensional two-band systems ($M = 2$) in the transpose-type time-reversal symmetry (class AII[†]). The symmetry imposes the constraint

$$U_T \mathcal{T}_N[h]^\top U_T^{-1} = \mathcal{T}_N[h], \quad (19)$$

where U_T is a unitary matrix. Using the non-Bloch representation and the convention in Eqs. (6), where transpose reverses the Laurent powers, the symmetry condition becomes

$$U_T h^\top (\beta^{-1}) U_T^{-1} = h(\beta^{-1}). \quad (20)$$

This symmetry constrains the polynomial $\det \sigma(\beta)$ to satisfy

$$\det \sigma(\beta) = \det \sigma(\beta^{-1}), \quad (21)$$

and hence it factorizes as

$$\det \sigma(\beta) = C_E \beta^{-2p} \prod_{j=1}^{2p} [\beta - \beta_j(E)][\beta - \beta_j^{-1}(E)]. \quad (22)$$

We order the β_j by modulus as

$$|\beta_{2p}^{-1}| \leq \dots \leq |\beta_1^{-1}| \leq 1 \leq |\beta_1| \leq \dots \leq |\beta_{2p}|, \quad (23)$$

so that each pair (β_j, β_j^{-1}) encodes a Kramers pair.

Class AIII[†] is characterized by the \mathbb{Z}_2 topological invariant [5] defined by

$$\begin{aligned} (-1)^{\nu[\tau]} &= \text{sgn} \left[\frac{\text{Pf } \tau(-1)}{\text{Pf } \tau(1)} \right. \\ &\times \left. \exp \left\{ -\frac{1}{2} \int_0^\pi dk \partial_k \ln \det \tau(e^{ik}) \right\} \right], \quad (24) \end{aligned}$$

with $\tau = (E - h)U_T$. The sign function, $\text{sgn}(x)$, takes the value +1 for $x > 0$ and -1 for $x < 0$, and $\text{Pf}[A]$ corresponds to the Pfaffian of the skew-symmetric matrix A .

The Ronkin function for class AIII[†] is compactly expressed as

$$R_\sigma(\mu) = \ln |C_E| - 2p\mu + \sum_{j=1}^{2p} [\max(\mu, \mu_j) + \max(-\mu, \mu_j)], \quad (25)$$

where $\mu_j = \ln |\beta_j| \geq 0$.

In the \mathbb{Z}_2 -nontrivial phase, two Kramers-related eigenstates localize on opposite edges with inverse localization lengths $\pm\mu_1$. Consequently, their contributions compete in the minimization in Eq. (14) and the conventional optimization formalism cannot be used.

To resolve this competition, we introduced the symmetry-decomposed Ronkin functions $R_\sigma^{(\pm)}$ in Ref. [91]. We impose that the decomposed Ronkin functions $R_\sigma^{(\pm)}$ inherit the key mathematical properties of R_σ , namely convexity, piecewise linearity, and integer-quantized derivatives. Moreover, $R_\sigma^{(\pm)}$ should satisfy the symmetry relations

$$R_\sigma(\mu) = R_\sigma^{(+)}(\mu) + R_\sigma^{(-)}(\mu), \quad R_\sigma^{(+)}(\mu) = R_\sigma^{(-)}(-\mu), \quad (26)$$

and remain consistent with the GBZ condition for class AIII[†] systems [48], where $R_\sigma^{(+)}$ is optimized within the interval $[\mu_1, \mu_2]$.

Under these assumptions, the symmetry-resolved

Ronkin functions take the forms:

$$\begin{aligned} R_\sigma^{(+)}(\mu) &= \frac{1}{2} \ln |C_E| - \frac{1}{2} \sum_{j=1}^{2p} \mu_j - \mu \\ &+ \sum_{j=1}^{2\pi} \max(\mu, \mu_j) \quad (27) \end{aligned}$$

$$\begin{aligned} R_\sigma^{(-)}(\mu) &= \frac{1}{2} \ln |C_E| + \frac{1}{2} \sum_{j=1}^{2p} \mu_j - (2p-1)\mu \\ &+ \sum_{j=1}^{2p} \max(-\mu, \mu_j). \quad (28) \end{aligned}$$

The contributions from the roots, the third and fourth term in Eq. (25), are distributed symmetrically between $R_\sigma^{(+)}$ and $R_\sigma^{(-)}$, whereas the pole contribution $-2p\mu$ is split asymmetrically for consistency with the GBZ condition.

Optimizing yields the OBC spectral potential

$$\phi(E) = \begin{cases} \min_\mu R_\sigma(\mu) & \nu[\tau] = 0 \\ 2 \min_\mu R_\sigma^{(+)}(\mu) & \nu[\tau] = 1 \end{cases} \quad (29)$$

which can be written compactly as

$$\phi(E) = \ln |C_E| + (-1)^{\nu[\tau]} \mu_1 + \sum_{j=2}^{2p} \mu_j. \quad (30)$$

The \mathbb{Z}_2 invariant determines the sign of the leading root's contribution, flipping the μ_1 term between the topologically trivial and nontrivial phases. This formulation reproduces the correct OBC spectral potential.

However, the above discussion relies on phenomenological intuition about assigning Kramers pairs to different decomposed functions, rather than on a rigorous mathematical basis. In particular, the applicability criteria of the generalized Szegő limit theorem in multiband systems have not been established, and the connection to this theorem therefore remains unclear. This lack of a mathematical foundation prevents the extension of the Amoeba formulation to general multiband class A systems.

III. WIENER-HOPF FACTORIZATION AND ITS APPLICATION TO BAND TOPOLOGY

In this section, we introduce the Wiener-Hopf factorization (WHF) and clarify its connection to the band topology of both Hermitian and non-Hermitian systems. We first review the WHF of matrix-valued Laurent polynomials arising from Hermitian Bloch Hamiltonians and summarize its established correspondence with band topology [92]. We then extend this framework to non-Hermitian Hamiltonians by employing the Hermitian doubling approach [4, 5], thereby demonstrating how the WHF naturally captures the topological structure of non-Hermitian bands.

A. Wiener-Hopf factorization for matrix Laurent polynomials

In this section, we consider a matrix-valued Laurent polynomial $A(\beta) = \sum_{j=-p}^q a_j \beta^j$, defined on the Riemann sphere $\mathbb{C} \cup \{\infty\}$.

A Wiener-Hopf factorization of A is a decomposition of the form

$$A(\beta) = A_+(\beta)D(\beta)A_-(\beta). \quad (31)$$

where the factors are given by

$$A_+(\beta) = \sum_{j=0}^q a_{+,j} \beta^j, \quad A_-(\beta) = \sum_{j=-p}^0 a_{-,j} \beta^j \quad (32)$$

and

$$D(\beta) = \text{diag}(\beta^{\kappa_1}, \dots, \beta^{\kappa_M}). \quad (33)$$

Here, $A_+(\beta)$ must be invertible for $|\beta| \leq 1$ (including the origin), while $A_-(\beta)$ must be invertible for $|\beta| \geq 1$ (including ∞). The integers κ_j are the partial indices of A , and we order them in descending order. We denote the set of partial indices of a symbol σ as

$$\mathcal{K}[\sigma] = (\kappa_1, \dots, \kappa_M). \quad (34)$$

We note that a WHF of A exists if and only if $A(\beta)$ is invertible on the unit circle, that is, $\det A(\beta) \neq 0$ for $|\beta| = 1$. This condition ensures that $\det A(\beta)$ has no zeros on the unit circle, so that analytic continuations of A_+ and A_- can be defined uniquely up to an invertible constant matrix. The factorization is not unique. Given an invertible matrix $U(\beta)$ with $\det U(\beta) = \text{const}$, another valid factorization can be found as

$$\begin{aligned} A_+DA_- &= (A_+U)D(D^{-1}U^{-1}DA_-) \\ &= A'_+DA'_-, \end{aligned} \quad (35)$$

where $A'_+ = A_+U$ and $A'_- = D^{-1}U^{-1}DA_-$. However, after fixing an ordering of the partial indices $\{\kappa_j\}$, the diagonal factor D is unique, so that the partial indices are uniquely defined.

We will often partition the index set $\{1, \dots, M\}$ into M_+ , M_0 , and M_- corresponding to positive, zero, and negative partial indices, respectively. The corresponding partial indices are referred as \mathcal{K}_+ , \mathcal{K}_0 , and \mathcal{K}_- .

B. Symmetric Wiener-Hopf factorization of Bloch Hamiltonians and band topology

We now consider the WHF of Hermitian Bloch Hamiltonians. As recently shown in Ref. [92], a modified WHF, referred to as the symmetric Wiener-Hopf factorization (SWHF), is closely related to band topology. Motivated by applications to non-Hermitian topology, we focus on

classes AIII and DIII, although analogous statements hold for other symmetry classes.

For a gapped Hermitian Bloch Hamiltonian, $h(\beta)$ admits a WHF

$$h(\beta) = h_+(\beta)\Lambda(\beta)h_-(\beta), \quad (36)$$

which can be chosen to respect Hermiticity,

$$h_+^\dagger = h_-, \quad \Lambda^\dagger = \Lambda. \quad (37)$$

As defined in Eq. (6), the Hermitian conjugation reverses the signs of the partial indices, $\kappa_j \mapsto -\kappa_j$. Together with the uniqueness of the partial indices, this implies that the set of partial indices of σ , denoted $\mathcal{K}[\sigma]$, is symmetric, so that every $\kappa_m > 0$ has a corresponding partner $-\kappa_m$. Thus, we can arrange Λ in a symmetric form

$$\begin{cases} \Lambda_{M+1-m,m} = \beta^{\kappa_m} & m \in M_+ \\ \Lambda_{m,M+1-m} = \beta^{-\kappa_m} & m \in M_+ \\ \Lambda_{m,m} = s_m & m \in M_0 \end{cases} \quad (38)$$

with $s_m \in \pm 1$ arranged in ascending order. Here, the block assignment realizes a symmetric placement of positive/negative indices. This type of factorization is called the symmetric Wiener-Hopf factorization (SWHF)[92].

In the presence of additional symmetries, the SWHF assumes a symmetry-constrained (modified) form. A Hamiltonian in class AIII satisfies the chiral symmetry, which allows h to be written as

$$h = \begin{pmatrix} 0 & A^\dagger \\ A & 0 \end{pmatrix}. \quad (39)$$

Then, the WHF of A , $A = A_+DA_-$, yields a SWHF of h in the form of

$$\begin{aligned} h &= h_+\Lambda h_- \\ &= \begin{pmatrix} A_-^\dagger & \\ & A_+ \end{pmatrix} \begin{pmatrix} D & \\ & D^\dagger \end{pmatrix} \begin{pmatrix} A_+ & \\ & A_-^\dagger \end{pmatrix}, \end{aligned} \quad (40)$$

consistent with Eq. (37).

Similarly, Hamiltonians in class DIII are block off-diagonal and admit an SWHF structurally equivalent to the AIII form introduced in Eq. (40). Time-reversal and particle-hole symmetries, however, constrain A to satisfy $A = -A^\top$ in an appropriate basis. Choosing a suitable U , as introduced in Eq. (35), we can determine the factors as,

$$A_+^\top = A_-, \quad D^\top = -D, \quad (41)$$

where D takes the skew-symmetric form

$$\begin{cases} D_{M+1-m,m} = -\beta^{\kappa_m} & m \in M_+ \\ D_{m,M+1-m} = \beta^{-\kappa_m} & m \in M_+ \\ D_{M+1-m,m} = 1 & m \in M_0, m \leq M/2 \\ D_{m,M+1-m} = -1 & m \in M_0, m \leq M/2 \end{cases} \quad (42)$$

Concrete algorithms for constructing both WHF and SWHF are provided in the Appendix of Ref. [92].

1. SWHF and Hermitian band topology

As demonstrated in Ref. [92], the SWHF of a Hermitian Bloch Hamiltonian is directly related to its band topology via the partial indices. For both classes AIII and DIII, the relevant topological invariants can be expressed in terms of the off-diagonal block A introduced in Eq. (39).

For class AIII, the topological invariant is the winding number of A . Considering the WHF $A = A_+ D A_-$, the factors A_+ and A_- are analytic and invertible for $|\beta| \leq 1$ and $|\beta| \geq 1$, respectively. Since A_{\pm} have neither zeros nor poles in their corresponding regions, their winding numbers vanish, $W[A_{\pm}] = 0$. Consequently, the winding number of A equals that of D ,

$$W[A] = W[D] = \sum_{\kappa \in \mathcal{K}[A]} \kappa. \quad (43)$$

Hence, the winding number is given by the sum of the partial indices. Furthermore, the number of right [left] localized modes is equivalent to the sum of positive [negative] partial indices.

Similarly, the \mathbb{Z}_2 topological invariant for class DIII is reduced by the WHF in Eqs. (41) and (42) to

$$(-1)^{\nu[A]} = \frac{\text{Pf } D(-1)}{\text{Pf } D(1)} = (-1)^{\sum_{\kappa \in \mathcal{K}_+[A]} \kappa}. \quad (44)$$

Here, we used $\det D = 1$ and $\text{Pf}(A_+ D A_+^\top) = (\det A_+) \text{Pf } D$. Therefore, the \mathbb{Z}_2 invariant is determined by the parity of the sum of the positive partial indices.

In both classes, the topological invariant is thus encoded in the partial indices of the off-diagonal block A .

2. WHF and non-Hermitian band topology

The WHF framework can also be applied to non-Hermitian Hamiltonians. Their topological classification can be carried out through Hermitization, i.e., by classifying the doubled Hermitian Hamiltonian at a reference energy E [4, 5].

A class A non-Hermitian Hamiltonian maps to a class AIII Hermitian Hamiltonian via Hermitization,

$$\tilde{\sigma} = \begin{pmatrix} & \sigma^\dagger \\ \sigma & \end{pmatrix}, \quad (45)$$

where $\sigma = E - h$. Therefore, a WHF of σ induces an SWHF of $\tilde{\sigma}$, and the topological information of σ is encoded in its partial indices.

A class AII[†] non-Hermitian Hamiltonian is mapped to a class DIII Hermitian Hamiltonian, with

$$\tilde{\tau} = \begin{pmatrix} & \tau^\dagger \\ \tau & \end{pmatrix}, \quad (46)$$

where $\tau = (E - h)U_T$. Therefore, the topological information can be obtained from the partial indices of τ .

IV. STRONG SZEGÖ LIMIT THEOREM AND WHF

In this section, we consolidate the theoretical groundwork connecting the Szegő limit theorem and the Wiener-Hopf factorization (WHF) as a preparation for our later analysis of multiband non-Hermitian systems. We first revisit the classical and modified Szegő limit theorems, interpreting them in terms of the partial indices of the WHF. This review clarifies the conditions under which the OBC and PBC spectral potentials coincide and identifies how nonvanishing partial indices lead to deviations in the OBC potential. These insights then form the basis for our generalization of the Szegő limit theorem to multiband systems in the following section.

A. Classical strong Szegő limit theorem and partial indices

Let σ be a matrix-valued Laurent polynomial (Hermitian or non-Hermitian). The classical strong Szegő limit theorem [88–90] concerns the asymptotic behavior of the determinant ratio E_N ,

$$\lim_{N \rightarrow \infty} E_N[\sigma] = \lim_{N \rightarrow \infty} \frac{\det \mathcal{T}_N[\sigma]}{G[\sigma]^{N+1}}, \quad (47)$$

where $G[\sigma]$ is the exponential of the Ronkin function for $\mu = 0$, corresponding to the PBC spectral potential. It is written as

$$G[\sigma] = \exp \left[\int_0^{2\pi} \frac{dk}{2\pi} \ln \det \sigma(e^{ik}) \right] = e^{R_\sigma(0)}. \quad (48)$$

This limit converges when σ is gapped on the unit circle and its winding number vanishes. Thus, the OBC spectral potential can be expressed as

$$\frac{1}{N} \ln \det \mathcal{T}_N[\sigma] = \frac{N+1}{N} R_\sigma(0) + \frac{1}{N} \ln E_N[\sigma], \quad (49)$$

indicating that its deviation from the PBC spectral potential is controlled by $E_N[\sigma]$. The applicability of the Szegő limit theorem can be expressed in terms of the partial indices of the WHF of σ [89]. When all partial indices of σ vanish, the ratio $E_N[\sigma] \rightarrow C \neq 0$ converges to a nonzero constant, and the OBC and PBC spectral potentials coincide up to $\mathcal{O}(1/N)$ corrections. Deviations from this condition arise when one or more partial indices are nonzero, in which case $E_N[\sigma]$ in Eq. (47) decays to zero, and the OBC and PBC spectral potentials no longer coincide. In this case, the convergence rate of $E_N[\sigma]$,

$$E_N[\sigma] = e^{-\alpha N + \mathcal{O}(N)}, \quad (50)$$

determines the deviation of the OBC potential by $-\alpha$ [93]. The convergence rate α is related to the localization length μ , on which we will focus later.

For single-band Hamiltonians, the winding number equals the partial index. Thus, optimizing the Ronkin function is equivalent to finding a μ for which the partial index of σ_μ is zero, and thus

$$\lim_{N \rightarrow \infty} \frac{1}{N} \ln \det \mathcal{T}_N[\sigma] = \min_{\mu} R_{\sigma}(\mu). \quad (51)$$

This is the generalized Szegő limit theorem proposed in Ref. [83].

In multiband systems, however, the total winding number is the sum of all partial indices, so a vanishing winding number no longer guarantees that each index individually vanishes. Consequently, the naive Amoeba formulation can fail unless there exists a μ for which all partial indices become zero. If such a μ exists, the classical Szegő limit theorem still holds for σ_μ ; otherwise, the correspondence between OBC and PBC potentials breaks down.

B. Modified Szegő limit theorem for topologically nontrivial Hermitian systems

As a next step, we review the modified Szegő limit theorem established for topologically nontrivial Hermitian Hamiltonians [92, 93], which governs the convergence behavior of $E_N[\sigma]$. We further summarize how these deviations are connected to boundary modes in such systems, thereby establishing the conceptual bridge used in the following section.

Let $\tilde{\sigma}$ be a Hermitian two-band class AIII Hamiltonian, written in the off-diagonal form of Eq. (39). Because of chiral symmetry, the winding number of the full Hamiltonian satisfies $W[\tilde{\sigma}] = 0$. However, the topology of $\tilde{\sigma}$ is characterized by the winding number of its off-diagonal block, $W[A] = \kappa$. When $\kappa = 0$, the system is topologically trivial and the determinant ratio $E_N[\tilde{\sigma}]$ converges to a finite, nonzero constant, as predicted by the classical Szegő limit theorem. For $\kappa \neq 0$, the Hamiltonian is topologically nontrivial, and $\mathcal{K}[\tilde{\sigma}]$ is $(|\kappa|, -|\kappa|)$. The resulting decay of $E_N[\tilde{\sigma}]$ to zero reflects the contribution of boundary-localized modes in $\mathcal{T}_N[\tilde{\sigma}]$.

It has been shown in Ref. [93] that the spectrum of $\mathcal{T}_N[\tilde{\sigma}]$ is well approximated by the PBC spectrum together with a pair of boundary-localized modes. However, due to finite-size hybridization, these two edge modes acquire small but finite energies $\pm\varepsilon$ rather than lying exactly at zero. The splitting ε scales with the overlap between the edge modes, $\varepsilon \propto e^{-\mu N}$, where $\mu > 0$ is the inverse localization length. The modified Szegő limit theorem [93] then implies

$$E_N[\tilde{\sigma}] \propto \varepsilon^2 \propto e^{-2\mu N}. \quad (52)$$

The generalization to multiple pairs of edge modes is straightforward by

$$E_N[\tilde{\sigma}] \propto \prod_j e^{-2\mu_j N}, \quad (53)$$

where $\mu_j > 0$ denotes the inverse localization lengths of each pair.

As discussed in Ref. [92], the number of zero modes is determined by $\mathcal{K}[\sigma]$. A positive partial index of $\mathcal{K}[A]$ corresponds to a mode localized at the right boundary, while a negative partial index of $\mathcal{K}[A]$ (or equivalently, a positive partial index of $\mathcal{K}[A^\dagger]$) corresponds to a mode localized at the left boundary.

For example, if $\kappa = 1$ (i.e., $W[A] = 1$), the off-diagonal block A contributes one right-localized mode, while A^\dagger contributes one left-localized mode. Thus, the full Hamiltonian $\mathcal{T}_N[\tilde{\sigma}]$ hosts one mode on each boundary. The localization length of these modes is determined by the root of $\det A$ with the largest magnitude inside the unit circle, yielding $\mu = \ln |\beta|$. This shows that the Szegő limit theorem for a topologically nontrivial Hermitian Hamiltonian must be modified by this decay exponent.

This argument extends to general nonzero κ . For positive (negative) κ , the block A contributes κ right- (left-) localized modes, governed by the κ roots of $\det A$ inside (outside) the unit circle with the largest (smallest) magnitudes. In either case, the total decay exponent is given by the sum of their inverse localization lengths.

The above discussion illustrates how nonzero winding numbers modify the asymptotic behavior of $E_N[\tilde{\sigma}]$. To further clarify the role of partial indices in multiband settings, we next consider a four-band class AIII Hamiltonian where the off-diagonal block A is a two-band matrix. In this case, even when $W[A] = 0$, the block A may still have nontrivial partial indices, e.g., $\mathcal{K}[A] = (+1, -1)$. Since $\tilde{\sigma}$ is constructed from A and A^\dagger , the partial indices $(+1, -1)$ of A lead to $\mathcal{K}[\tilde{\sigma}] = (+1, +1, -1, -1)$ for the full Hamiltonian $\tilde{\sigma}$. Thus, A supports two edge modes localized at opposite boundaries, and $\mathcal{T}_N[\tilde{\sigma}]$ hosts two pairs of edge modes in total. These modes are controlled by the dominant roots of $\det A$: one root β_2 with the smallest absolute value outside the unit circle and one root β_1 with the largest absolute value inside. We denote their inverse localization lengths as $\mu_2 = \ln |\beta_2| > 0$ and $\mu_1 = \ln |\beta_1| < 0$, respectively. The contribution to $E_N[\tilde{\sigma}]$ then becomes

$$E_N[\tilde{\sigma}] \propto e^{-2\mu_2 N} e^{2\mu_1 N} = e^{-2(\mu_2 - \mu_1) N}. \quad (54)$$

We note that $\mu_2 - \mu_1$ is equivalent to the length of the interval where $W[\sigma_\mu]$ vanishes.

V. AMOEBA FORMULATION FOR MULTIBAND SYSTEMS VIA WHF

Building on the theoretical groundwork developed in the previous sections, we extend the Amoeba framework by incorporating the WHF to treat non-Hermitian systems with nonzero partial indices through Hermitian doubling. This formulation unifies the analytic structure of the Amoeba with the topological information encoded in the WHF, leading to a generalized Szegő limit theorem for multiband non-Hermitian systems. Focusing

on class AIII[†], we further show that the WHF naturally gives rise to the symmetry-decomposed Ronkin function proposed in our previous work [91], thereby providing a rigorous foundation for the generalized Szegő relation in time-reversal-symmetric non-Hermitian systems.

A. Correction for non-vanishing partial indices for class A

We now extend the preceding discussion to topologically nontrivial non-Hermitian Hamiltonians and derive the Generalized Szegő limit theorem with non-vanishing partial indices.

In non-Hermitian systems, topological phases often manifest not through isolated edge states but through the extensive localization of bulk modes near the boundaries, as seen in the NHSE. Through Hermitian doubling, each localized non-Hermitian bulk mode corresponds to a quasi-zero mode of a doubled Hermitian Hamiltonian with the same localization length [16, 21]. This correspondence enables us to apply the modified Szegő limit theorem established for Hermitian systems to derive a generalized version valid for non-Hermitian Hamiltonians.

We first validate this approach in a single-band system and confirm that it reproduces the known results of the conventional Amoeba formulation. As an illustrative example, let σ be a non-Hermitian symbol whose determinant factorizes as

$$\det \sigma(\beta) = C\beta^{-p} \prod_{j=1}^{p+q} [\beta - \beta_j], \quad (55)$$

where $\beta_1, \dots, \beta_{p+1}$ are inside the unit circle ($|\beta_j| < 1$), and $\beta_{p+2}, \dots, \beta_{p+q}$ are outside the circle ($|\beta_j| > 1$). This root distribution corresponds to a winding number $W[\sigma] = 1$. The corresponding Hermitianized symbol $\tilde{\sigma}$ is defined in Eq. (45) and belongs to a two-band class AIII system. The edge mode of this Hamiltonian is governed by $\mu_{p+1} (< 0)$, which implies $E_N[\tilde{\sigma}] = \exp[2\mu_{p+1}N]$ [Eq. (52)]. Using the relation $E_N[\tilde{\sigma}] = |E_N[\sigma]|^2$, the modified Szegő limit theorem for $\tilde{\sigma}$ yields the deviation for the potential of σ :

$$\begin{aligned} \lim_{N \rightarrow \infty} \frac{1}{N} \ln |\det \mathcal{T}_N[\sigma]| &= R_\sigma(0) + \mu_{p+1} \\ &= \ln |C| + \sum_{j=p+1}^{p+q} \mu_j, \end{aligned} \quad (56)$$

which reproduces the generalized Szegő limit theorem for $W[\sigma] = 1$. This argument straightforwardly generalizes to arbitrary winding numbers, corresponding to the optimization form in Eq. (51).

This framework for evaluating potential deviations, based on the asymptotic behavior of $E_N[\tilde{\sigma}]$, naturally extends to multiband systems with non-vanishing partial indices. As another illustrative example, consider a

two-band symbol σ with vanishing total winding number $W[\sigma] = 0$ but nonzero partial indices $\mathcal{K}[\sigma] = (1, -1)$. Let $\det \sigma$ factorize as

$$\det \sigma(\beta) = C\beta^{-2p} \prod_{j=1}^{2(p+q)} [\beta - \beta_j], \quad (57)$$

where $\beta_1, \dots, \beta_{2p}$ lie inside the unit circle ($|\beta_j| < 1$) and $\beta_{2p+1}, \dots, \beta_{2(p+q)}$ lie outside it ($|\beta_j| > 1$). This choice ensures $W[\sigma] = 0$. Using the asymptotic form of $E_N[\tilde{\sigma}]$ for the $(+1, -1)$ index structure, Eq. (54), we obtain

$$\lim_{N \rightarrow \infty} \frac{1}{N} \ln |\det \mathcal{T}_N[\sigma]| = R_\sigma(0) - (\mu_{2p+1} - \mu_{2p}), \quad (58)$$

where $\mu_{2p} = \ln |\beta_{2p}|$ is the logarithmic radius of the largest roots inside the unit circle and $\mu_{2p+1} = \ln |\beta_{2p+1}|$ that of the smallest root outside.

It is instructive to interpret the correction term in Eq. (58) from a "local" perspective using the roots of $\det \sigma$ as Eq. (17). For $W[\sigma] = 0$, the PBC spectral potential $R_\sigma(0)$ is given by the sum over roots outside the unit circle, $\ln |C| + \sum_{j=2p+1}^{2(p+q)} \mu_j$. The OBC spectral potential $\phi(E)$ in Eq. (58) thus becomes:

$$\phi(E) = \ln |C| + \mu_{2p} + \sum_{j=2p+2}^{2(p+q)} \mu_j \quad (59)$$

Thus, the contribution from the smallest outside root (μ_{2p+1}) is removed and replaced by that of the largest inside root (μ_{2p}). This result offers a clear interpretation: the nonvanishing partial indices quantify how many root contributions are exchanged across the unit circle. In this example, $\mathcal{K}[\sigma] = (1, -1)$ means that, even though $W[\sigma] = 0$, the correct OBC potential involves one such exchange, where the positive index brings in the innermost interior root and the negative index removes the outermost exterior root.

Finally, we generalize this result to the case with a nonzero winding number, $W[\sigma] \neq 0$. Since the OBC determinant is invariant under the similarity transformation in Eq. (12), we can eliminate the winding number $W[\sigma_\mu]$ by introducing an appropriate shift μ . This allows us to apply Eq. (58) using the roots of $\det \sigma_\mu$. Therefore, we obtain a modified form of Eq. (51) that accounts for the nonvanishing partial indices $(1, -1)$:

$$\lim_{N \rightarrow \infty} \frac{1}{N} \ln |\det \mathcal{T}_N[\sigma]| = \min_{\mu} R_\sigma(\mu) - (\mu_{k+1} - \mu_k), \quad (60)$$

where μ_k and μ_{k+1} denote, respectively, the dominant roots located just inside and just outside the circle of radius e^μ .

Building on the above observation, the validity of the Amoeba formulation is determined by the behavior of the partial indices after optimization. We therefore introduce the residual partial indices,

$$\mathcal{K}^*[\sigma] \equiv \mathcal{K}[\sigma_{\mu^*}], \quad (61)$$

defined as the set of partial indices evaluated at the optimal shift μ^* , chosen such that the global winding number vanishes, $W[\sigma_{\mu^*}] = 0$.

If, at this optimum, all residual partial indices vanish individually, $\mathcal{K}^* = (0, 0, \dots)$, the conventional Amoeba optimization remains valid and the generalized Szegő limit theorem applies. However, when one or more residual indices are nonzero, the simple Amoeba formulation breaks down, and the generalized Szegő limit theorem must include additional correction terms determined by \mathcal{K}^* . Consequently, the generalized Szegő limit theorem takes the compact form

$$\lim_{N \rightarrow \infty} \frac{1}{N} \ln |\det \mathcal{T}_N[\sigma]| = \mathcal{M}_{\mathcal{K}^*}[\sigma], \quad (62)$$

where $\mathcal{M}_{\mathcal{K}^*}[\sigma]$ depends on the residual partial indices as

$$\mathcal{M}_{(0,0)}[\sigma] = \min_{\mu} R_{\sigma}(\mu), \quad (63)$$

$$\mathcal{M}_{(+1,-1)}[\sigma] = \min_{\mu} R_{\sigma}(\mu) - (\mu_{k+1} - \mu_k). \quad (64)$$

B. Generalized Szegő limit theorem for class AII[†]

We now demonstrate that the WHF of a non-Bloch Hamiltonian in the two-band class AII[†] naturally leads to a decomposition of the Ronkin function, yielding the symmetry-decomposed forms defined in Eqs. (27) and (28).

1. WHF and symmetry-decomposed Ronkin functions

We focus on two-band ($M = 2$) class AII[†] systems. Here, we define the total Ronkin function and its symmetry-decomposed counterparts using $\tau = (E - h)U_T$ instead of $\sigma = E - h$. Since U_T is a unitary matrix, R_{τ} is equivalent to R_{σ} . This redefinition aligns more naturally with the WHF framework for class AII[†] systems, enabling a symmetric decomposition of the Ronkin function.

As established in Sec. III B, the topological information is encoded in the partial indices of τ . The SWHF of τ can be arranged as shown in Eq. (41),

$$\tau = \tau_+ D_{\kappa} \tau_-, \quad (65)$$

where $\tau_+^{\top} = \tau_-$ and D_{κ} takes a form given by Eq. (42),

$$D_{\kappa=0} = \begin{pmatrix} & -1 \\ 1 & \end{pmatrix} \quad \text{or} \quad D_{\kappa>0} = \begin{pmatrix} & \beta^{-\kappa} \\ -\beta^{\kappa} & \end{pmatrix}. \quad (66)$$

We distinguish between the cases where the partial indices are $(0, 0)$ and $(+\kappa, -\kappa)$ with $\kappa > 0$. The \mathbb{Z}_2 invariant can be evaluated as

$$(-1)^{\nu[\tau]} = (-1)^{\kappa}. \quad (67)$$

Thus, the parity of κ determines the \mathbb{Z}_2 invariant.

We can rewrite the SWHF of τ , Eq. (65), in a symplectic form

$$\tau = \tau_+^{\text{symp}} J \tau_-^{\text{symp}}, \quad \tau_+^{\text{symp}} = \tau_+ S_{\kappa}, \quad \text{and} \quad J = \begin{pmatrix} & 1 \\ -1 & \end{pmatrix}. \quad (68)$$

Here, $[\tau_+^{\text{symp}}]^{\top} = \tau_-^{\text{symp}}$. The factor S_{κ} appearing in τ_+^{symp} , takes the form

$$S_{\kappa=0} = \begin{pmatrix} & 1 \\ 1 & \end{pmatrix} \quad \text{or} \quad S_{\kappa>0} = \begin{pmatrix} \beta^{-\kappa} & \\ & 1 \end{pmatrix}. \quad (69)$$

Using this factorization, we now define the decomposed Ronkin functions:

$$R_{\tau}^{(+)}(\mu) = \int_0^{2\pi} \frac{dk}{2\pi} \ln \left| \det [\tau_+^{\text{symp}}]_{\mu} \right| \quad (70)$$

$$R_{\tau}^{(-)}(\mu) = \int_0^{2\pi} \frac{dk}{2\pi} \ln \left| \det [\tau_-^{\text{symp}}]_{\mu} \right|. \quad (71)$$

These quantities correspond to the contributions from τ_+^{symp} and τ_-^{symp} sectors, respectively. This WHF-based definition is applicable regardless of the topological phase, providing a unified framework.

Furthermore, this formulation is consistent with the phenomenological construction in Eqs. (27) and (28). Since $\det J = 1$, it follows that

$$\det \tau = \det(\tau_+^{\text{symp}}) \det(\tau_-^{\text{symp}}) \quad (72)$$

Considering $\tau_+^{\text{symp}}[\tau_-^{\text{symp}}]$ has neither roots nor poles inside [outside] the unit circle, we find that

$$\det(\tau_+^{\text{symp}}) = \sqrt{C_E \prod_{j=1}^{2p} \beta_j^{-1} \times \beta^{-\kappa} \prod_{j=1}^{2p} [\beta - \beta_j]} \quad (73)$$

$$\det(\tau_-^{\text{symp}}) = \sqrt{C_E \prod_{j=1}^{2p} \beta_j \times \beta^{\kappa-2p} \prod_{j=1}^{2p} [\beta - \beta_j^{-1}]}. \quad (74)$$

By integrating these expressions, we obtain the symmetry-decomposed Ronkin functions $R_{\tau}^{(\pm)}$, recovering the forms given in the Eqs. (27) and (28) for the cases where $\kappa = 0$, and 1.

2. WHF and generalized Szegő limit theorem for class AII[†]

We now provide a proof of the generalized Szegő limit theorem for class AII[†] using the WHF-based Ronkin functions.

The TRS[†] operator U_T is independent of β , which implies that $\mathcal{T}_N[U_T]$ is diagonal. Accordingly, the OBC spectral potential $\phi(E)$ can be rewritten as

$$\phi(E) = \lim_{N \rightarrow \infty} \frac{1}{N} \ln |\det \mathcal{T}_N[\sigma]| = \lim_{N \rightarrow \infty} \frac{1}{N} \ln |\det \mathcal{T}_N[\tau]|. \quad (75)$$

Using the symplectic form of the WHF, Eq. (68), the spectral potential can be decomposed as

$$\phi(E) = \frac{2}{N} \ln |\det \mathcal{T}_N[\tau_+^{\text{symp}}]| + \frac{1}{N} \ln |\det \mathcal{T}_N[J]| + \mathcal{O}(N^{-1}). \quad (76)$$

The symplectic factor J does not contribute to the leading term since $\det \mathcal{T}_N[J] = (\det J)^N = 1$. The factor τ_+^{symp} itself does not preserve TRS^\dagger symmetry, since it corresponds to only one sector of the full WHF and therefore lacks the full symmetric structure. The Kramers-paired roots have been separated into τ_+^{symp} and τ_-^{symp} .

For $\kappa = 0$, τ_+ is invertible inside the unit circle, and $\tau_+^{\text{symp}} = \tau_+ S_0$ shares the same analytic domain. Thus, τ_+^{symp} admits a trivial WHF, $\tau_+^{\text{symp}} = \tau_+ S_0 \cdot 1 \cdot 1$, where both the central factor D and the right factor A_- are the identity, so all partial indices of τ_+^{symp} vanish. Consequently, the classical Szegő limit theorem applies directly to the symbol τ_+^{symp} :

$$\phi(E) = 2 \int_0^{2\pi} \frac{dk}{2\pi} \ln |\det \tau_+^{\text{symp}}| = \int_0^{2\pi} \frac{dk}{2\pi} \ln |\det \tau|. \quad (77)$$

For $\kappa > 0$, the factor S_κ contains negative powers of β . The WHF of $\tau_+^{\text{symp}} = \tau_+ S_\kappa$ takes the form $\tau_+^{\text{symp}} = \tau_+ \cdot S_\kappa \cdot 1$, where the central factor is S_κ , and hence $\mathcal{K}[\tau_+^{\text{symp}}] = (0, -\kappa)$. Consequently, we must apply the generalized Szegő limit theorem, Eq. (62), which accounts for these nonzero partial indices

$$\phi(E) = 2\mathcal{M}_{\mathcal{K}^*}[\tau_+^{\text{symp}}], \quad (78)$$

where \mathcal{K}^* denotes the residual partial indices of τ_+^{symp} , i.e., the partial indices of the similarity-transformed symbol $[\tau_+^{\text{symp}}]_\mu(e^{ik}) = \tau_+^{\text{symp}}(e^{\mu+ik})$ evaluated at the optimally chosen μ for which the total winding vanishes. If the partial indices of $[\tau_+^{\text{symp}}]_\mu$ vanish simultaneously, i.e., the residual partial indices are trivial, $\mathcal{K}^*[\tau_+^{\text{symp}}] = (0, 0)$, the simple optimization formulation is recovered:

$$\phi(E) = 2\mathcal{M}_{(0,0)}[\tau_+^{\text{symp}}] = 2 \min_\mu R_\tau^{(+)}. \quad (79)$$

If the partial indices of the optimized $[\tau_+^{\text{symp}}]_\mu$ do not vanish simultaneously, i.e., $\mathcal{K}^*[\tau_+^{\text{symp}}] = (-1, 1)$, the optimal value must be corrected according to Eq. (62):

$$\phi(E) = 2\mathcal{M}_{(+1,-1)}[\tau_+^{\text{symp}}] = 2(\min_\mu R_\tau^{(+)}(\mu) - (\mu_{k+1} - \mu_k)), \quad (80)$$

where μ_k and μ_{k+1} denote, respectively, the dominant roots of τ_+^{symp} located just inside and just outside the circle of radius e^μ .

Combining the results for $\kappa = 0$ and $\kappa > 0$, we arrive at a unified expression for the OBC spectral potential, valid for all $\kappa \geq 0$:

$$\phi(E) = 2\mathcal{M}_{\mathcal{K}^*}[\tau_+^{\text{symp}}] \quad (81)$$

This expression reproduces Eq. (29) for $\kappa = 0$ and 1, and extends it naturally to higher topological sectors ($\kappa \geq 2$).

VI. NUMERICAL VERIFICATION

In this section, we validate the WHF-based formulation developed in the preceding sections. First, we analyze class-A two-band systems with nonvanishing partial indices and examine the correction to the generalized Szegő limit theorem. We show that nonzero partial indices invalidate the simple optimization formalism, and that the necessary correction is given by Eq. (62). Next, we verify the WHF-based decomposition of the Ronkin function for systems with TRS^\dagger , considering two representative parameter sets. We demonstrate that the WHF-based decomposed Ronkin functions reproduce the phenomenological symmetry-decomposed Ronkin functions in the regions where $\kappa = 0$ and 1. Finally, we investigate the parameter regime where a $\kappa = 2$ domain emerges.

A. Correction for non-vanishing partial indices in two-band class A systems

In this section, we numerically verify the correction to the generalized Szegő limit theorem that arises from nonvanishing partial indices, Eq. (62). Our aim is to demonstrate a situation in which the conventional Amoeba formulation fails, thereby necessitating the correction term derived in Sec. V.

To this end, we consider a model in which there is a parameter regime, where the partial indices $\mathcal{K}[\sigma_\mu]$ do not simultaneously vanish for any shift μ . The simplest example with this property is a block-diagonal two-band Hamiltonian composed of two uncoupled Hatano-Nelson chains:

$$\begin{cases} h(\beta) &= \begin{pmatrix} h_1(\beta) & \\ & h_2(\beta) \end{pmatrix} \\ h_1(\beta) &= 1.3\beta^{-1} - 0.2 + 0.7\beta \\ h_2(\beta) &= 0.5\beta^{-1} + 0.3 + 0.1i + 1.5\beta \end{cases} \quad (82)$$

We define the symbols of the blocks as $\sigma_{1,2} = E - h_{1,2}$ and the full symbol as $\sigma = \text{diag}(\sigma_1, \sigma_2)$. The partial indices of the full system, $\mathcal{K}[\sigma] = (\kappa_1, \kappa_2)$, are then given simply by the winding numbers of the uncoupled blocks, $\kappa_{1,2} = W[\sigma_{1,2}]$.

Figure 1 depicts the topological phases in the complex energy plane, showing the PBC (blue dotted lines) and OBC (red lines) spectra. The shaded regions indicate where the partial indices (winding numbers) take nonzero values. In the blue-shaded area, $\mathcal{K}[\sigma] = (-1, 0)$; in the red-shaded area, $\mathcal{K}[\sigma] = (0, 1)$. The overlap between them, shown in purple, marks the regime where $\mathcal{K}[\sigma] = (-1, 1)$, in which the conventional Amoeba formulation fails and the generalized correction becomes essential. In the white region where $\mathcal{K}[\sigma] = (0, 0)$, the PBC and OBC potentials coincide, and the conventional Amoeba formulation holds.

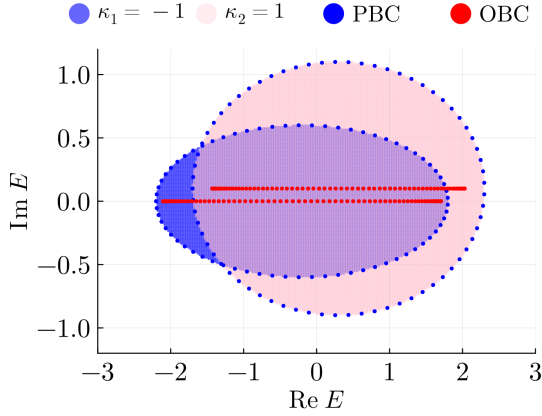


FIG. 1: Comparison of OBC and PBC spectra for the two uncoupled Hatano-Nelson models defined in Eq. (82). Blue dotted lines show the PBC spectra of the individual blocks h_1 and h_2 , while red lines denote the full OBC spectrum for $N = 70$. Shaded regions in the complex energy plane indicate where the partial indices are nonzero. The blue-shaded region corresponds to $\kappa_1 = W[\sigma_1] = -1$ with $\kappa_2 = 0$, and the red-shaded region corresponds to $\kappa_2 = W[\sigma_2] = 1$ with $\kappa_1 = 0$. Their overlap (purple) represents the regime $\mathcal{K}[\sigma] = (-1, 1)$, where the conventional Amoeba optimization breaks down and the generalized formulation of Sec. V must be applied.

Figure 2 verifies our theoretical prediction by analyzing the optimization landscape at two representative reference energies E for the Hamiltonian defined in Eq. (82). The panels show the Ronkin functions R_σ (black), R_{σ_1} (red), and R_{σ_2} (orange), with vertical gray dashed lines marking the root positions μ_j . Fig. 2(a) shows the trivial case at $E = -2.0 + 1.0i$ where the partial indices vanish simultaneously, i.e., $\mathcal{K}[\sigma] = (0, 0)$. Fig. 2(b) shows the nontrivial case at $E = 0.0 + 0.2i$ where the partial indices do not vanish simultaneously, i.e., $\mathcal{K}[\sigma] = (-1, 1)$. We note that since the winding number $W[\sigma]$ vanishes at both points, the conventional optimization formulation predicts the OBC potential as $R_\sigma(0)$.

For the case $E = -2.0 + 1.0i$ [Fig. 2(a)], the reference point lies in the white region of Fig. 1, and $\mathcal{K}[\sigma] = (0, 0)$. The Ronkin functions R_{σ_1} and R_{σ_2} admit a common minimization interval, so the simple optimization scheme applies. In contrast, for $E = 0.0 + 0.2i$ [Fig. 2(b)], the reference point lies in the purple region with nonzero partial indices, $\mathcal{K}[\sigma] = (-1, 1)$. As a result, there is no region where the Ronkin functions R_{σ_1} and R_{σ_2} can be jointly minimized, signaling the breakdown of the simple optimization scheme and requiring the correction term in Eq. (62). For this specific model and parameter set, the correction term evaluates to $-(\mu_3 - \mu_2)$, corresponding to the modification $\min_\mu R_\sigma(\mu) - (\mu_{k+1} - \mu_k)$ in Eq. (62). This correction accounts for the exchange of contributions between the largest inner root (μ_2) and the smallest

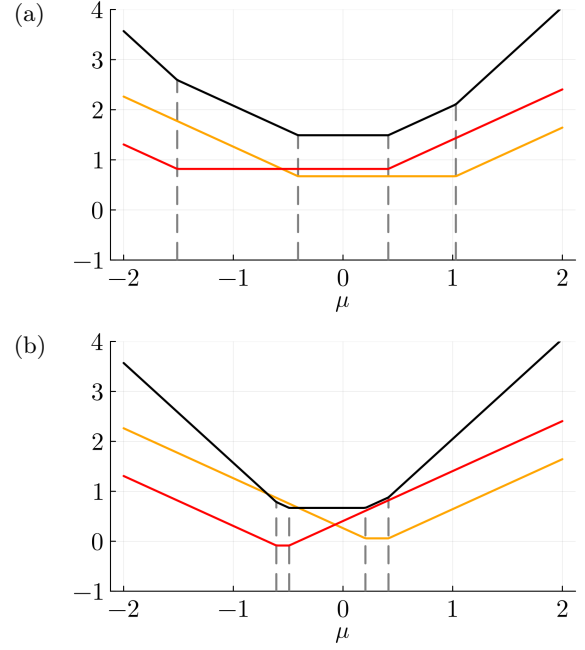


FIG. 2: Ronkin functions for two representative reference energies E , selected from distinct topological domains in Fig. 1. The total Ronkin function R_σ is shown in black, while the partial Ronkin functions R_{σ_1} and R_{σ_2} are plotted in red and orange, respectively. (a) Trivial case ($E = -2.0 + 1.0i$): The reference point lies in the white region, where $\mathcal{K}[\sigma] = (0, 0)$. Both R_{σ_1} and R_{σ_2} can be minimized simultaneously, and the conventional optimization scheme applies. (b) Nontrivial case ($E = 0.0 + 0.2i$): The reference point lies in the purple region, where $\mathcal{K}[\sigma] = (-1, 1)$. Here, R_{σ_1} and R_{σ_2} cannot be minimized simultaneously, and the correction term in Eq. (62) is required to obtain the correct OBC potential.

outer root (μ_3) at the minimum of R_σ .

The above discussion extends to points with non-vanishing winding number $W[\sigma] \neq 0$ by employing the similarity transformation and using μ -dependent partial indices $\mathcal{K}[\sigma_\mu] = (\kappa_1^{(\mu)}, \kappa_2^{(\mu)})$. Figure 3 illustrates this for two instructive reference energies from the red region in Fig. 1. In addition to the Ronkin functions, we show the partial indices $\kappa_1^{(\mu)}$ (red) and $\kappa_2^{(\mu)}$ (orange) separately. For $E = 2.2 + 0.1i$ [Fig. 3(a)], the partial indices share a common vanishing interval; equivalently, the residual partial indices vanish $\mathcal{K}^*[\sigma] = (0, 0)$. In this case, the simple optimization scheme applies, and the minimum of $R_\sigma(\mu)$ correctly yields the OBC potential. For the case $E = 0.5 + 0.6i$ [Fig. 3(b)], the partial indices never vanish simultaneously for any μ , so $\mathcal{K}^*[\sigma] = (+1, -1)$, and the correction in Eq. (62) is necessitated.

To test our prediction quantitatively, we compute the DOS, using the residual partial indices as a guide to determine where the correction term must be applied. Figure 4 compares the DOS obtained from (a) the conven-

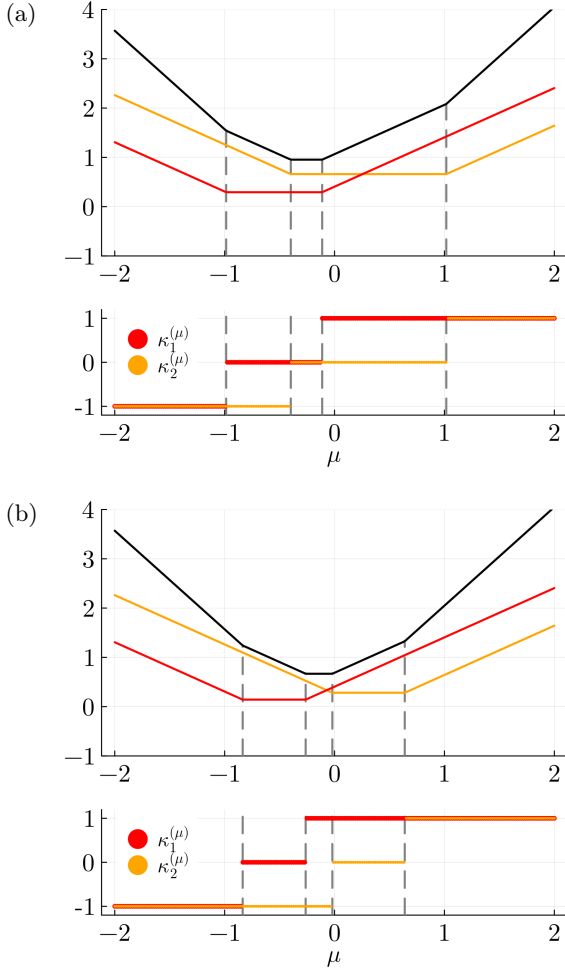


FIG. 3: Ronkin functions and μ -dependent partial indices for two reference energies taken from the red region in Fig. 1. Each top panel shows the Ronkin functions, similar to Fig. 2. Each bottom panel displays the μ -dependent partial indices $\mathcal{K}[\sigma_\mu] = (\kappa_1^{(\mu)}, \kappa_2^{(\mu)})$. (a) $E = 2.2 + 0.1i$: The partial indices vanish after optimization, i.e., the residual partial indices are $\mathcal{K}^*[\sigma] = (0, 0)$, yielding the correct OBC potential through the standard optimization scheme. (b) $E = 0.5 + 0.6i$: The residual partial indices are nonzero even after optimization, $\mathcal{K}^*[\sigma] = (+1, -1)$, indicating that the correction in Eq. (62) is required to obtain the correct potential.

tional simple optimization and (b) our WHF-based formulation [Eq. (62)]. Because of the discretization of the Hessian in Eq. (8), the plotted values are scaled by the energy cell area $\Delta \text{Re } E \times \Delta \text{Im } E \simeq 2.5 \times 10^{-4}$. As shown in Fig. 4(a), the simple optimization fails to reproduce the OBC DOS. By contrast, the corrected WHF-based formulation [Fig. 4(b)] accurately reproduces the OBC DOS, in excellent agreement with the spectrum shown in Fig. 1.

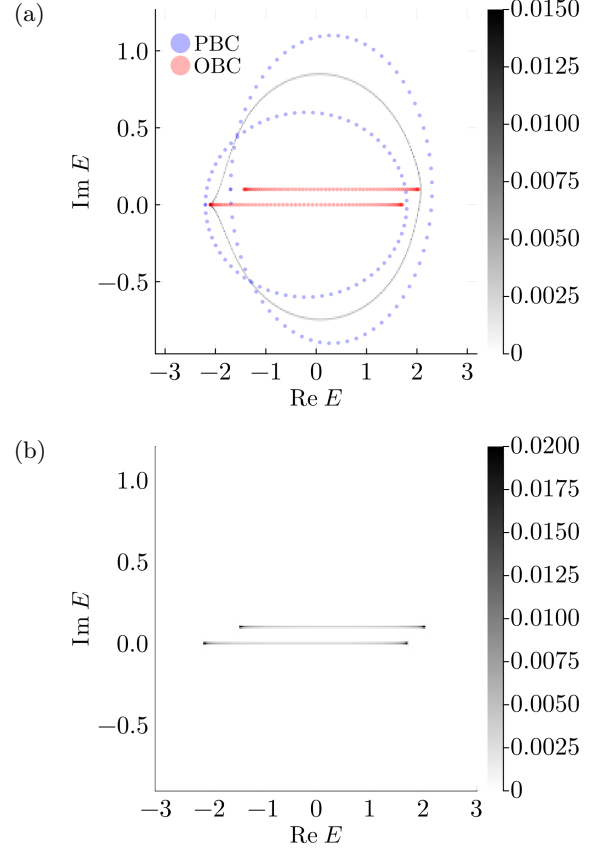


FIG. 4: Comparison of the DOS evaluated by (a) the conventional formulation and (b) our WHF-based formulation. Values are scaled by the area of the energy cell $\Delta \text{Re } E \times \Delta \text{Im } E \simeq 2.5 \times 10^{-4}$ due to the discretizations of the Hessian in Eq. (8). (a) The conventional simple optimization fails to reproduce the OBC spectrum (red line), as evident from the mismatch with the calculated DOS (grayscale). (b) The WHF-based formulation, which includes the correction for nonvanishing partial indices, accurately reproduces the OBC spectrum.

B. WHF framework in systems with TRS^\dagger

Next, we verify the WHF-based decomposition for class AIII^\dagger in one dimension, by analyzing the two-band symplectic Hatano-Nelson model with next-nearest-neighbor hopping for two different parameter sets. The first set corresponds to the model previously studied in Ref. [91]. We demonstrate that the WHF-based decomposition of the Ronkin function reproduces the symmetry-decomposed form introduced in that work, confirming the consistency of the two approaches.

The non-Bloch Hamiltonian is given by

$$h(\beta) = (t_2 - i\Delta_2 X + g_2 Z)\beta^{-2} + (t_1 - i\Delta_1 X + g_1 Z)\beta^{-1} + (t_1 + i\Delta_1 X - g_1 Z)\beta + (t_2 + i\Delta_2 X - g_2 Z)\beta^2 \quad (83)$$

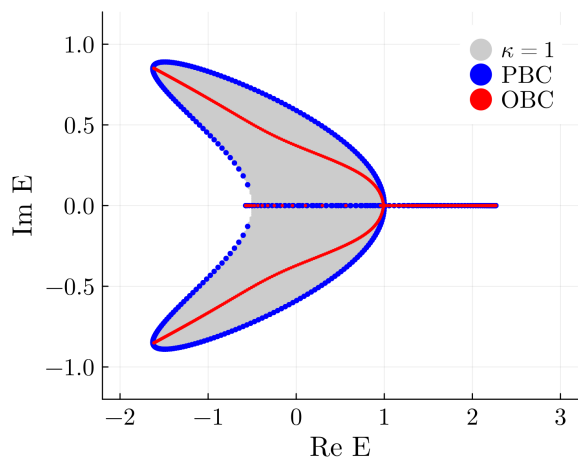


FIG. 5: Validation of the partial index κ as the topological invariant. The Hamiltonian is defined in Eq. (83), with parameters $t_1 = 0.3$, $t_2 = 0.8$, $g_1 = 0.5$, $\Delta_1 = 0.3$, and $\Delta_2 = 0.2$. Blue and red points indicate the PBC and OBC spectra, respectively ($N = 400$). The shaded region denotes the domain where the WHF-derived partial index is $\kappa = 1$. This region coincides with the \mathbb{Z}_2 -nontrivial phase ($\nu[\tau] = 1$) obtained independently, confirming that the parity of κ correctly captures the \mathbb{Z}_2 topology.

where X, Y, Z are Pauli matrices. The TRS^\dagger operator is iY , which is independent of β , consistent with Eq. (6).

1. Regime with $\kappa = 0, 1$

First, we confirm that the WHF-based formalism reproduces the symmetry-decomposed Ronkin function for parameters yielding the positive partial index as $\kappa = 0$ or 1. The parameters are set to $t_1 = 0.3$, $t_2 = 0.8$, $g_1 = 0.5$, $\Delta_1 = 0.3$, and $\Delta_2 = 0.2$.

In this parameter regime, the system is characterized by the \mathbb{Z}_2 topological invariant $\nu[\tau]$, where $\tau = (E - h)U_T$, Eq. (24) [5]. As established in Sec. III B, $\nu[\tau]$ is equivalent to the parity of the sum of positive partial indices. Figure 5 shows the positive partial index κ of $\tau = (E - h)U_T$ across the complex energy plane. Blue and red points indicate the PBC and OBC spectra, respectively, obtained by diagonalizing the Hamiltonian with 400 sites. This model exhibits two distinct phases: $\kappa = 0$ (white) and $\kappa = 1$ (shaded). The shaded $\kappa = 1$ region coincides with the topologically nontrivial region identified by the \mathbb{Z}_2 topological invariant [91]. This confirms that the parity of κ provides a consistent and physically equivalent characterization of the \mathbb{Z}_2 topology in class AII † systems.

Having confirmed that κ serves as the correct topological index, we now verify the central mechanism of our WHF formulation [Eq. (81)], which defines the OBC potential through the symplectic form of the WHF,

$\tau = \tau_+ S_\kappa J [\tau_+ S_\kappa]^\top$, as given in Eq. (68). Figure 6 illustrates this test for three representative energies E . The top row [Fig. 6(a-c)] presents the WHF-based decomposed Ronkin functions $R_\tau^{(\pm)}$, while the bottom row [Fig. 6(d-f)] shows the corresponding partial indices of $[\tau_+^{\text{symp}}]_\mu = [\tau_+ S_\kappa]_\mu$. The reference points are chosen as $E = -0.5 + 0.3i$ ($\kappa = 1$) [(a,d)], $E = 0.5 + 0.265i$ ($\kappa = 1$) [(b,e)], and $E = 1.2 + 0.2i$ ($\kappa = 0$) [(c,f)]. The top panels (a-c) demonstrate that the WHF-derived $R_\tau^{(\pm)}$ perfectly reproduce the phenomenological decomposed Ronkin functions [Eqs. (27) and (28)]: they are convex, piecewise linear, and satisfy the symmetry relation $R_\tau^{(+)}(\mu) = R_\tau^{(-)}(-\mu)$ [Eq. (26)]. The bottom panels [Fig. 6(d-f)] display the partial indices $\mathcal{K}[[\tau_+^{\text{symp}}]_\mu] = (\kappa_1^{(\mu)}, \kappa_2^{(\mu)})$ of the factor $[\tau_+^{\text{symp}}]_\mu$. Their transposed counterparts follow $\mathcal{K}[[\tau_-^{\text{symp}}]_\mu] = (-\kappa_2^{(-\mu)}, -\kappa_1^{(-\mu)})$. Each index changes when μ crosses a root μ_j where τ closes its gap. The sum $\kappa_1^{(\mu)} + \kappa_2^{(\mu)}$ corresponds to the winding number of $[\tau_+^{\text{symp}}]_\mu$, which in turn equals the derivative of $R_\tau^{(+)}$.

Strikingly, we find that the partial indices $\kappa_{1,2}^{(\mu)}$ vanish simultaneously within the finite interval $\mu_1 \leq \mu \leq \mu_2$; thus, $\mathcal{K}^*[[\tau_+^{\text{symp}}]_\mu] = (0, 0)$. The emergence of this interval provides direct numerical evidence that the WHF framework is fully consistent with the non-Bloch band theory for class AII † systems: it coincides precisely with the optimization window $[\mu_1, \mu_2]$ dictated by the GBZ condition [48]. From the perspective of the formulation based on the WHF, the condition $\mathcal{K}^*[[\tau_+^{\text{symp}}]_\mu] = (0, 0)$ precisely marks the regime in which the generalized Szegő limit theorem [Eq. (79)] holds exactly, without requiring any additional correction terms.

Finally, as a comprehensive validation of our framework, we compute the OBC spectral DOS by evaluating the OBC potential through the WHF-based optimization [Eq. (70)] across the entire complex energy plane. The resulting distribution is shown in Fig. 7, where each point represents an energy cell of size $\Delta \text{Re } E \times \Delta \text{Im } E \simeq 4 \times 10^{-4}$, used for discretizing the Hessian in Eq. (8). The WHF-based decomposition accurately reproduces the OBC spectrum, in full agreement with Fig. 5 and consistent with the results obtained from the symmetry-decomposed Ronkin functions. This excellent correspondence confirms both the validity and the practical applicability of our method across the $\kappa = 0$ and $\kappa = 1$ regimes.

2. Regime including $\kappa = 2$

To demonstrate that Eq. (81) also holds in parameter regimes with partial index $\kappa = 2$, we analyze the same Hamiltonian using parameters $t_1 = 0.3$, $t_2 = 0.5$, $g_2 = 1.0$, $\Delta_1 = 0.0$, and $\Delta_2 = 0.9$.

Figure 8 shows the spectrum and partial index in the complex energy plane. The blue and red points denote

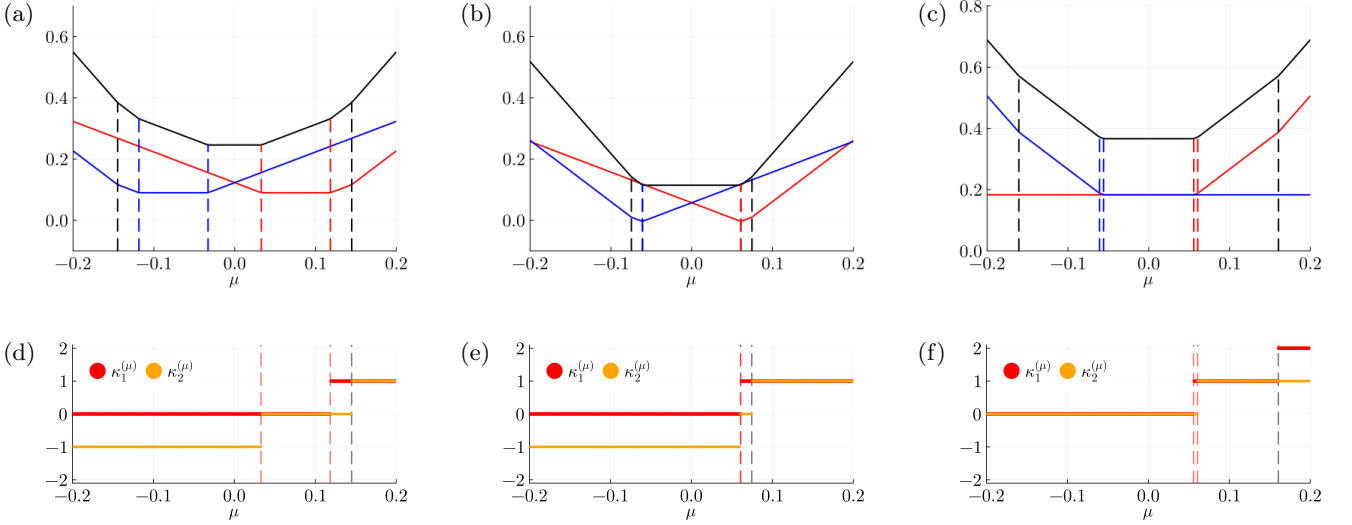


FIG. 6: WHF-based decomposed Ronkin functions (top row, a-c) and partial indices of $[\tau_+^{\text{symp}}]_\mu$, $\mathcal{K}[[\tau_+^{\text{symp}}]_\mu] = (\kappa_1^{(\mu)}, \kappa_2^{(\mu)})$ (bottom row, d-f). The panels correspond to three reference energies: (a, d) $E = -0.5 + 0.3i$ ($\kappa = 1$), (b, e) $E = 0.5 + 0.265i$ ($\kappa = 1$), and (c, f) $E = 1.2 + 0.2i$ ($\kappa = 0$). (a-c): decomposed Ronkin functions $R_\tau^{(+)}$ (red), $R_\tau^{(-)}$ (blue), and total R_τ (black). Vertical dashed lines mark the root positions $\mu = \pm\mu_j$, where the colored lines correspond to the GBZ condition $\mu_1 = \mu_2$. Due to TRS^\dagger , R_τ is even in μ , and $R_\tau^{(\pm)}$ obey the symmetry relation in Eq. (26). (d-f): partial indices $\kappa_1^{(\mu)}$ (red) and $\kappa_2^{(\mu)}$ (orange), which change whenever μ crosses a root μ_j where σ_μ closes its gap. Their sum, $\kappa_1^{(\mu)} + \kappa_2^{(\mu)}$, equals the derivative of $R_\tau^{(+)}$. The WHF-based decomposition reproduces the phenomenological symmetry-decomposed Ronkin functions for $\kappa = 1$ and symmetrically decomposition R_τ for $\kappa = 0$.

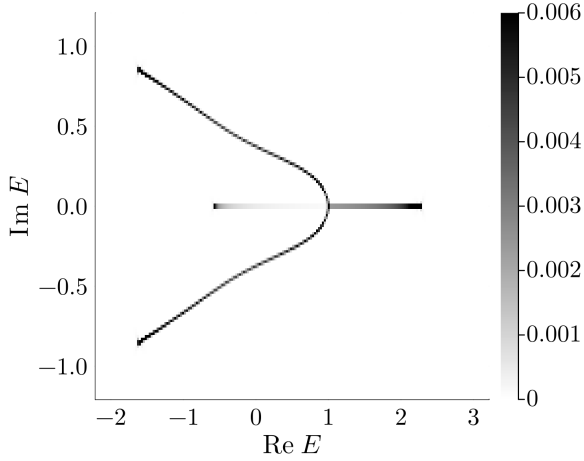


FIG. 7: DOS multiplied by $\Delta \text{Re } E \times \Delta \text{Im } E \simeq 4 \times 10^{-4}$, calculated by optimizing the WHF-based decomposed Ronkin functions defined in Eq (70). The Hamiltonian and parameters are equivalent to those in Fig. 5. The WHF-based formulation reproduces the OBC spectrum shown in Fig. 5.

the PBC and OBC spectra, respectively, obtained using $N = 200$ (PBC) and $N = 50$ (OBC) sites. The partial index κ of $\tau = (E - h)U_T$ takes the value 1 in the light-gray region, 2 in the dark-gray region, and 0 elsewhere.

Because the numerical diagonalization of this two-band Hamiltonian under OBC becomes increasingly demanding with system size, we restrict the calculation to 50 sites for the OBC case, which still captures the essential spectral features.

Crucially, in the $\kappa = 2$ region (dark gray), the \mathbb{Z}_2 topological invariant [Eq. (24)] yields $\nu[\tau] = 0$, implying topological triviality from the \mathbb{Z}_2 viewpoint. Yet, this regime reveals a previously unexplored structure: despite its \mathbb{Z}_2 -trivial character, the partial indices of the symbol remain nonzero, indicating the presence of exponentially localized states under OBC, as typically associated with the NHSE. This sets the $\kappa = 2$ phase apart from both the conventional trivial ($\kappa = 0$) and topological nontrivial ($\kappa = 1$) cases. Further evidence for the presence of a skin effect in this regime is provided by the OBC spectrum, which differs markedly from the PBC spectrum and shows pronounced boundary sensitivity. The combination of nonvanishing partial indices (signaling localization) and the pronounced boundary sensitivity of the OBC spectrum relative to the PBC spectrum provides clear evidence that a skin effect occurs in the $\kappa = 2$ regime. This skin effect is not protected by TRS^\dagger symmetry but instead originates from the nontrivial $\kappa = 2$ winding. The resulting $\kappa = 2$ skin modes are fragile: a small TRS^\dagger -preserving perturbation (e.g., $\Delta_1 = 0.01$) can remove them entirely without closing the point gap, confirming that these skin modes lack symmetry protec-

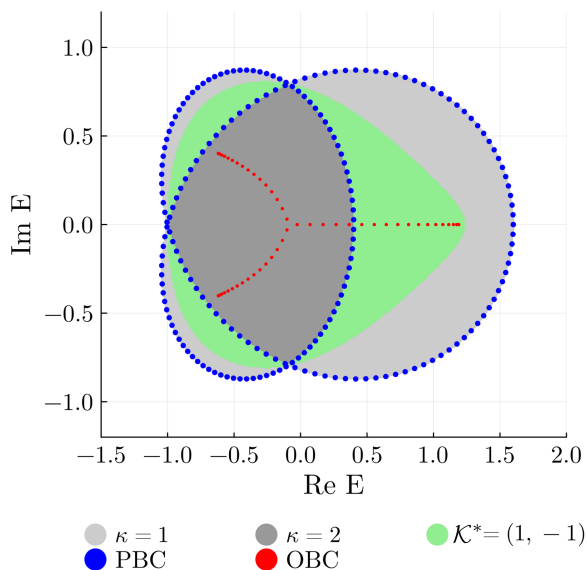


FIG. 8: Map of the OBC and PBC spectra with WHF-derived partial indices of the regime, including a $\kappa = 2$ phase. Blue and red points denote the PBC ($N = 200$) and OBC ($N = 50$) spectra, respectively. Model parameters are $t_1 = 0.3$, $t_2 = 0.5$, $g_2 = 1.0$, $\Delta_1 = 0.0$, and $\Delta_2 = 0.9$. The shaded regions indicate the WHF-derived partial index: $\kappa = 1$ (light gray) and, notably, a $\kappa = 2$ phase (dark gray). The unshaded (white) region corresponds to the trivial $\kappa = 0$ phase. The green overlay marks a parameter domain where the partial indices do not vanish simultaneously, leading to nonvanishing residual partial indices $\mathcal{K}^* = (+1, -1)$.

tion and arise solely from the winding structure. For further details, see Appendix A.

Having established the existence of the $\kappa = 2$ phase, we now examine the optimization of the factor $[\tau_+^{\text{symp}}]_\mu$ [from Eq. (68)], which plays a central role in decomposing the Ronkin function. Our WHF analysis reveals a complication: a parameter region where the partial indices of $[\tau_+^{\text{symp}}]_\mu$ do not vanish simultaneously, leaving residual partial indices $\mathcal{K}^*[\tau_+^{\text{symp}}] \neq (0, 0)$ even after finding the optimal μ , as indicated by the green area in Fig. 8. Within this green region, the optimization yields $\mathcal{K}^*[\tau_+^{\text{symp}}] = (1, -1)$ [or $(-1, 1)$], demonstrating that a straightforward optimization of the decomposed Ronkin function is insufficient and that a correction for the nonvanishing partial indices is required, analogous to the multiband class A case.

Figure 9 illustrates this behavior. The top panels [Fig. 9(a-c)] display the WHF-based decomposed Ronkin functions, while the bottom panels [Fig. 9(d-f)] show the μ -dependence of the partial indices, $\mathcal{K}[[\tau_+^{\text{symp}}]_\mu] = (\kappa_1^{(\mu)}, \kappa_2^{(\mu)})$. For reference points outside the green region in Fig. 8 [Figs. 9(a, c)], the decomposed Ronkin function $R_\tau^{(+)}$ (red line) is correctly minimized within the interval $[\mu_2, \mu_3]$, and the partial indices $\mathcal{K}[[\tau_+^{\text{symp}}]_\mu]$ vanish

simultaneously [Figs. 9(d, f)], confirming that the simple optimization formalism remains valid. In contrast, for energies inside the green region [Figs. 9(b, e)], no interval exists where the partial indices vanish simultaneously, necessitating the correction term in Eq. (62).

The resulting OBC DOS, multiplied by the surface element $\Delta \text{Re } E \times \Delta \text{Im } E \simeq 3 \times 10^{-4}$, is plotted in Fig. 10. The OBC potential is obtained by optimizing the decomposed Ronkin functions defined in Eq. (70), together with the correction in Eq. (80). By combining these two relations, the WHF-based formulation successfully reproduces the OBC spectrum shown in Fig. 8.

Our numerical analysis reveals that the conventional GBZ condition $\mu_1 = \mu_2$ [48] is replaced by $\mu_2 = \mu_3$. This modified GBZ condition is consistent with the WHF decomposed Ronkin functions and directly dictates the localization length of the eigenmodes. We interpret this behavior as a manifestation of the $\kappa = 2$ phase, which, as discussed in Appendix A, is generally fragile.

To verify the accuracy of the localization length, Fig. 11 shows fits of the OBC eigenstates ($N = 50$) using the functional form $e^{-\mu_2(x-25)} + e^{\mu_2(x-25)}$, where the values of $\mu_2 (= \mu_3)$ are obtained from the WHF-based optimization process. The red and blue lines represent the wave functions of the $+1$ and -1 sectors of the Pauli matrix Z , respectively. For $E = 1.02 + 0.06i$ [Fig. 11(b)], the partial index is $\kappa = 1$, and the corresponding eigenmode exhibits a TRS^\dagger -protected \mathbb{Z}_2 skin mode. In contrast, for $E = -0.13 + 0.08i$ [Fig. 11(a)], the partial index is $\kappa = 2$, and the corresponding eigenmode realizes a non-protected skin mode. The fitting form, based on the optimized μ_2 , accurately reproduces the spatial profiles in both regimes.

VII. CONCLUSION

In this work, we have established the Wiener-Hopf factorization (WHF) as a powerful framework for extending the Amoeba formulation to multiband non-Hermitian systems. Our approach resolves a key limitation of the existing formalism: although the generalized Szegő limit theorem is, in principle, valid in arbitrary dimensions, its practical application has been restricted to single-band systems due to complications arising from competing localization lengths in multiband settings, an effect that becomes unavoidable in the presence of symmetry-protected degeneracies.

By combining the WHF with Hermitian doubling, we have provided a clear physical interpretation of the generalized Szegő limit theorem: edge modes in the doubled Hermitian Hamiltonian generate the shift between the OBC and PBC spectral potentials. This perspective naturally identifies the precise criterion for the validity of the simple Amoeba optimization, i.e., that all residual partial indices must vanish. When this condition holds, the conventional generalized Szegő limit theorem applies directly; when it does not, we derived the corresponding

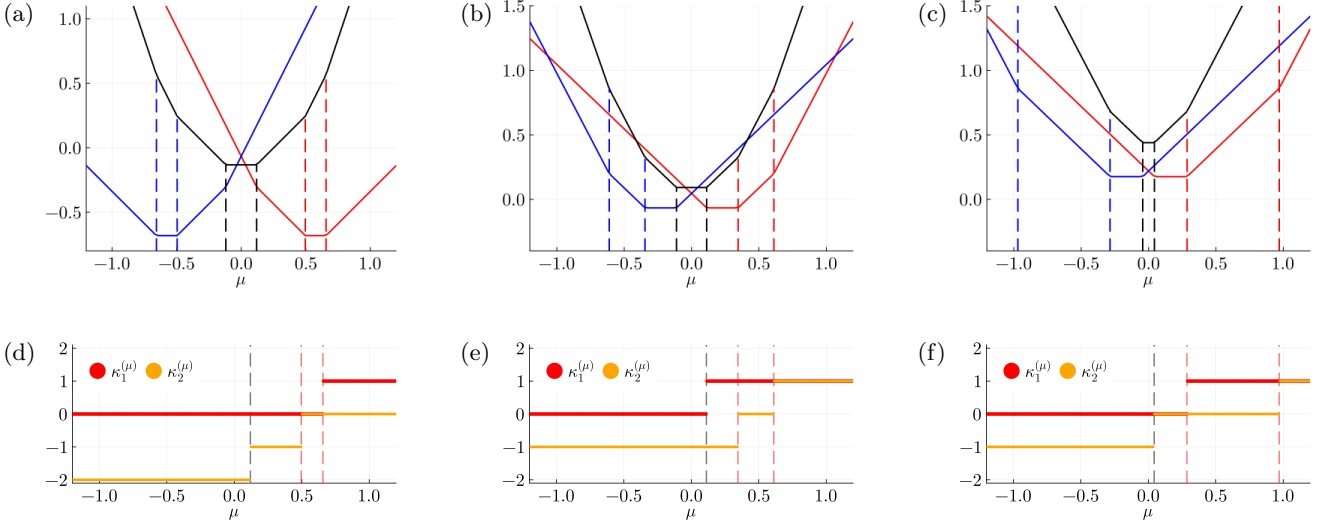


FIG. 9: Partial indices of $[\tau_+^{\text{symp}}]_\mu$ for three representative energies: (a) $E = -0.5 + 0.3i$ with $\kappa = 2$, (b) $E = 0.6 + 0.2i$ with $\kappa = 1$, and (c) $E = 0.9 + 0.7i$ with $\kappa = 1$. Red and blue vertical lines correspond to the GBZ condition $\mu_2 = \mu_3$. Outside the green region in Fig. 8 [(a), (c)], $\kappa_1^{(\mu)}$ and $\kappa_2^{(\mu)}$ vanish simultaneously for an appropriate μ , resulting in vanishing residual partial indices. Inside the green region [(b)], however, the partial indices never vanish simultaneously, indicating the breakdown of the simple optimization formalism due to nonvanishing residual partial indices.

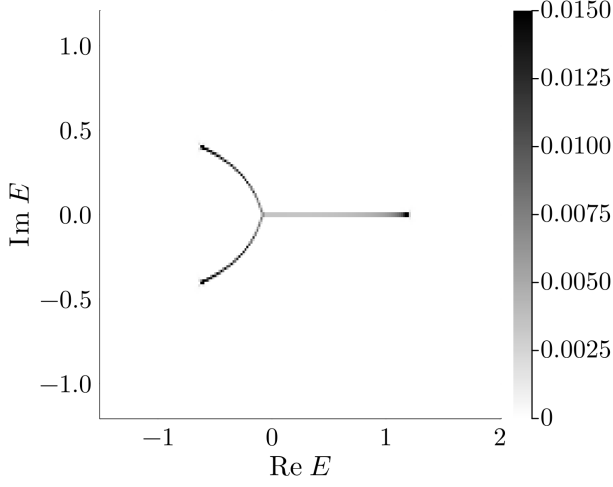


FIG. 10: Density of states (DOS) multiplied by the surface element $\Delta \text{Re } E \times \Delta \text{Im } E \simeq 3 \times 10^{-4}$. The Hamiltonian and parameters are identical to those in Fig. 8. The OBC spectral potential is obtained by optimizing the WHF-based decomposed Ronkin functions [Eq. (70)] together with the correction term accounting for nonvanishing partial indices [Eq. (80)]. The resulting WHF-based formulation accurately reproduces the OBC spectrum shown in Fig. 8.

correction terms [Eq. (62)], which account for the nonvanishing residual partial indices.

For systems with transpose-type time-reversal symmetry (class AIII[†]), we showed that the WHF naturally

yields the symmetry-decomposed Ronkin functions introduced phenomenologically in Ref. [91]. Through the symplectic form of the WHF [Eq. (68)], we obtain a rigorous decomposition $R_\tau(\mu) = R_\tau^{(+)}(\mu) + R_\tau^{(-)}(\mu)$, directly linking the WHF to the non-Bloch band theory. This decomposition is not merely a computational convenience but reflects the intrinsic structure of Kramers pairs in these systems.

Our WHF-based framework reveals a fundamental connection between the topological structure of non-Hermitian Hamiltonians and the asymptotic behavior of their OBC determinants. The partial indices, which encode the number and localization of boundary modes, directly control the deviations between OBC and PBC spectral potentials. This insight extends the modified Szegő limit theorem, originally formulated for Hermitian topological systems [93], into the non-Hermitian domain, as the generalized Szegő limit theorem [83]. The breakdown of the simple optimization formalism in multiband systems is thus not a deficiency but a natural manifestation of nontrivial topological structure. The required correction terms acquire a transparent physical interpretation: they describe the exchange of root contributions across the Brillouin zone boundary.

While this work focused on one-dimensional systems in classes A and AIII[†], the same mechanism is expected to extend to certain higher-dimensional cases [76], though its full generalization to higher dimensions remains an open challenge.

In conclusion, the Wiener-Hopf factorization provides a unified mathematical foundation for the Amoeba for-

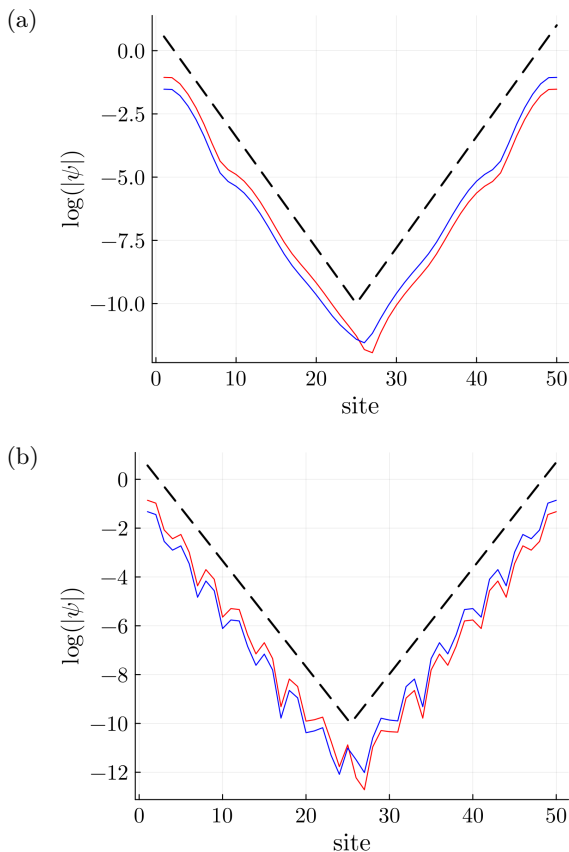


FIG. 11: Fitting of wave functions for (a) $\kappa = 1$ and (b) $\kappa = 2$. The chain length of the OBC system is $N = 50$ sites. The corresponding eigenenergies are (a) $E = 1.02 + 0.06i$ and (b) $E = -0.13 + 0.08i$. The red and blue lines represent the wave functions of the +1 and -1 sectors of the Pauli matrix Z , respectively. The black dotted line shows the fitted profile using the localization lengths determined from the optimization, corresponding to $\mu_2 = \mu_3$.

mulation in multiband systems, resolving long-standing questions about the applicability of the generalized Szegő limit theorem and establishing rigorous connections to non-Hermitian topology. This framework not only validates existing phenomenological approaches but also paves the way toward systematic extensions across symmetry classes and spatial dimensions.

ACKNOWLEDGEMENTS

S.K. deeply appreciates the fruitful discussions with D. Nakamura, K. Shimomura, and K. Kawabata. This work is supported by JSPS, KAKENHI Grants No. JP24KJ1353 (S.K.).

DATA AVAILABILITY

The data that support the findings of this article are not publicly available upon publication because it is not technically feasible and/or the cost of preparing, depositing, and hosting the data would be prohibitive within the terms of this research project. The data are available from the authors upon reasonable request.

APPENDIX

A. Instability of the $\kappa = 2$ phase and modified GBZ condition

In this Appendix, we examine the fragility of the $\kappa = 2$ phase in class AIII[†] and show that its apparent stability originates from an underlying unitary symmetry. This hidden symmetry enforces the modified GBZ condition $\mu_2 = \mu_3$, replacing the conventional relation $\mu_1 = \mu_2$.

The $\kappa = 2$ phase is inherently fragile. Within the framework of the Hermitian-doubled Hamiltonian, this phase corresponds to the presence of two Kramers pairs. As in the case of \mathbb{Z}_2 topological phases, an even number of Kramers pairs is not protected against generic TRS[†]-preserving perturbations: pairs can hybridize and gap out each other, rendering the phase topologically trivial.

In our model, this inherent fragility can explicitly be confirmed. The $\kappa = 2$ phase, which exists for $\Delta_1 = 0$, disappears upon introducing a TRS[†]-preserving perturbation $\Delta h(e^{ik}) = -2\Delta_1 X \sin k$, even for a small value $\Delta_1 = 0.01$, as shown in Fig. 12. Under this perturbation, the $\kappa = 2$ in the system changes to a $\kappa = 0$ phase without appreciable change in the PBC spectrum. The winding in the PBC spectrum remains unchanged, indicating that the underlying bulk topology of the PBC bands is unaffected.

This behavior can be understood by analyzing the symmetries of the unperturbed Hamiltonian $h(k)$ (i.e., for $\Delta_1 = 0$):

$$h(e^{ik}) = 2t_1 \cos k + 2t_2 \cos 2k - 2(\Delta_2 X + ig_2 Z) \sin 2k. \quad (84)$$

The Hamiltonian $h(k)$ can be diagonalized by a k -independent unitary matrix V ,

$$V^{-1}hV = \begin{pmatrix} h_+ & \\ & h_- \end{pmatrix}, \quad (85)$$

where each block is given by

$$h_{\pm}(e^{ik}) = 2t_1 \cos k + 2t_2 \cos 2k \pm 2iZ \sqrt{g_2^2 - \Delta_2^2} \sin 2k. \quad (86)$$

This diagonal form reveals an additional hidden unitary symmetry of the unperturbed Hamiltonian,

$$[h, VZV^{-1}] = 0. \quad (87)$$

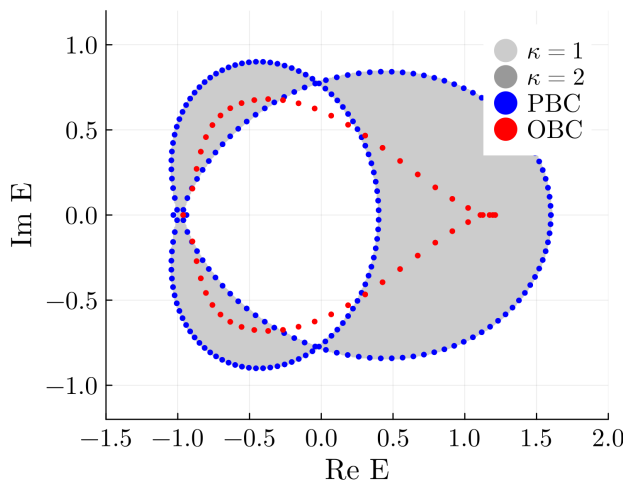


FIG. 12: Test of the stability of the $\kappa = 2$ phase under a TRS^\dagger -preserving perturbation. The parameters are identical to those in Fig. 8 except for $\Delta_1 = 0.01$. Introducing the perturbation $\Delta h(e^{ik}) = -2\Delta_1 X \sin k$ removes the $\kappa = 2$ phase, confirming its fragility. The original $\kappa = 2$ phase changes to a $\kappa = 0$ phase without any qualitative change in the PBC spectrum, indicating that the bulk winding of the PBC Hamiltonian remains unchanged.

Owing to this symmetry, the system decouples into two independent blocks h_+ and h_- , corresponding respectively to Kramers partners with partial indices $\pm\kappa = W[h_\pm]$. As a result, hybridization between the Kramers pairs is prohibited, which stabilizes the $\kappa = 2$ phase for these specific parameters.

The perturbation $\Delta h(e^{ik}) = -2\Delta_1 X \sin k$, however, breaks this hidden symmetry, since the perturbed Hamiltonian $h(e^{ik}) + \Delta h(e^{ik})$ can no longer be diagonalized by a k -independent matrix. As a consequence, the two Kramers pairs hybridize and gap each other out, leading to the disappearance of the $\kappa = 2$ phase. This demonstrates that the $\kappa = 2$ phase is not protected by TRS^\dagger alone but instead relies on the additional hidden unitary symmetry VZV^{-1} .

This hidden symmetry also drives the shift of the GBZ condition from the conventional $\mu_1 = \mu_2$ [48] to $\mu_2 = \mu_3$. The intrinsic instability of the $\kappa = 2$ phase underlies the emergence of the green region in Fig. 8, the parameter

domain where $\mathcal{K}^* = (1, -1)$ and whose boundary satisfies the conventional relation $\mu_1 = \mu_2$. In our specific model, both the $\kappa = 2$ phase and this $\mathcal{K}^* \neq (0, 0)$ region are stabilized by a hidden unitary symmetry. When a small TRS^\dagger -preserving perturbation breaks this symmetry, the $\kappa = 2$ phase disappears, and the OBC spectrum expands to the boundary of the green region, thereby restoring the standard GBZ condition. Thus, the nonvanishing partial indices and the accompanying ‘‘abnormal’’ GBZ relation ($\mu_2 = \mu_3$) are fragile artifacts of this hidden symmetry rather than a robust modification of the GBZ itself.

Figure 13 corroborates this discussion by showing the OBC DOS of the perturbed Hamiltonian, scaled by the surface element $\Delta \text{Re } E \times \Delta \text{Im } E \simeq 2 \times 10^{-4}$. Because the perturbation breaks the hidden symmetry, the conventional GBZ condition $\mu_1 = \mu_2$ is restored. Due to finite-size effects, the OBC spectrum obtained by direct diagonalization ($N = 50$, red dotted line) exhibits a small shift relative to the WHF-based results, which represent the $N \rightarrow \infty$ limit. Nevertheless, both results are consistent within the thermodynamic limit.

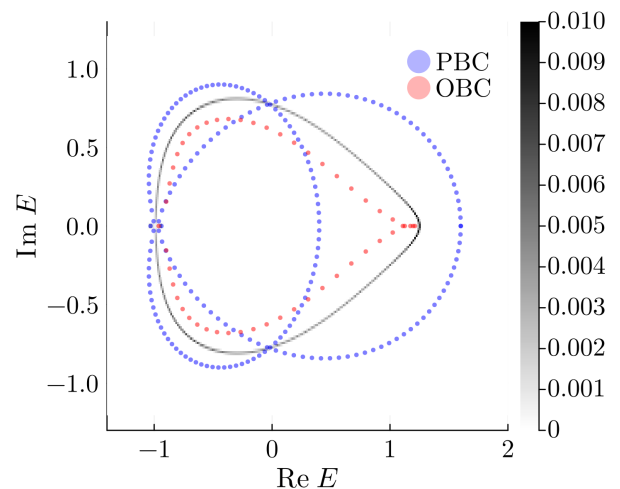


FIG. 13: DOS multiplies by surface element $\Delta \text{Re } E \times \Delta \text{Im } E \simeq 2 \times 10^{-4}$. The Hamiltonian and parameters are identical to those in Fig. 12. Due to the finite-size effect, the OBC spectrum shifts from the Amoeba results. However, these results coincide in the thermodynamic limit.

- [1] Yuto Ashida, Zongping Gong, and Masahito Ueda, ‘‘Non-hermitian physics,’’ *Advances in Physics* **69**, 249–435 (2020).
- [2] Emil J. Bergholtz, Jan Carl Budich, and Flore K. Kunst, ‘‘Exceptional topology of non-hermitian systems,’’ *Rev. Mod. Phys.* **93**, 015005 (2021).
- [3] Kun Ding, Chen Fang, and Guancong Ma, ‘‘Non-hermitian topology and exceptional-point geometries,’’

Nature Reviews Physics **4**, 745–760 (2022).

- [4] Zongping Gong, Yuto Ashida, Kohei Kawabata, Kazuaki Takasan, Sho Higashikawa, and Masahito Ueda, ‘‘Topological phases of non-hermitian systems,’’ *Phys. Rev. X* **8**, 031079 (2018).
- [5] Kohei Kawabata, Ken Shiozaki, Masahito Ueda, and Masatoshi Sato, ‘‘Symmetry and topology in non-hermitian physics,’’ *Phys. Rev. X* **9**, 041015 (2019).

- [6] Tony E. Lee, “Anomalous edge state in a non-hermitian lattice,” *Phys. Rev. Lett.* **116**, 133903 (2016).
- [7] Shunyu Yao and Zhong Wang, “Edge states and topological invariants of non-hermitian systems,” *Phys. Rev. Lett.* **121**, 086803 (2018).
- [8] Flore K. Kunst, Elisabet Edvardsson, Jan Carl Budich, and Emil J. Bergholtz, “Biorthogonal bulk-boundary correspondence in non-hermitian systems,” *Phys. Rev. Lett.* **121**, 026808 (2018).
- [9] Kazuki Yokomizo and Shuichi Murakami, “Non-bloch band theory of non-hermitian systems,” *Phys. Rev. Lett.* **123**, 066404 (2019).
- [10] Ching Hua Lee and Ronny Thomale, “Anatomy of skin modes and topology in non-hermitian systems,” *Phys. Rev. B* **99**, 201103 (2019).
- [11] Flore K. Kunst and Vatsal Dwivedi, “Non-hermitian systems and topology: A transfer-matrix perspective,” *Phys. Rev. B* **99**, 245116 (2019).
- [12] Fei Song, Shunyu Yao, and Zhong Wang, “Non-hermitian topological invariants in real space,” *Phys. Rev. Lett.* **123**, 246801 (2019).
- [13] M. Brandenbourger, X. Locsin, E. Lerner, and C. Coulais, “Non-reciprocal robotic metamaterials,” *Nat. Commun.* **10**, 4608 (2019).
- [14] Kai Zhang, Zhesen Yang, and Chen Fang, “Correspondence between winding numbers and skin modes in non-hermitian systems,” *Phys. Rev. Lett.* **125**, 126402 (2020).
- [15] Zhesen Yang, Kai Zhang, Chen Fang, and Jiangping Hu, “Non-hermitian bulk-boundary correspondence and auxiliary generalized brillouin zone theory,” *Phys. Rev. Lett.* **125**, 226402 (2020).
- [16] Nobuyuki Okuma, Kohei Kawabata, Ken Shiozaki, and Masatoshi Sato, “Topological origin of non-hermitian skin effects,” *Phys. Rev. Lett.* **124**, 086801 (2020).
- [17] Linhu Li, Ching Hua Lee, Sen Mu, and Jiangbin Gong, “Critical non-hermitian skin effect,” *Nat. Commun.* **11**, 5491 (2020).
- [18] Kohei Kawabata, Masatoshi Sato, and Ken Shiozaki, “Higher-order non-hermitian skin effect,” *Phys. Rev. B* **102**, 205118 (2020).
- [19] Stefano Longhi, “Non-bloch-band collapse and chiral zener tunneling,” *Phys. Rev. Lett.* **124**, 066602 (2020).
- [20] Tsuneya Yoshida, Tomonari Mizoguchi, and Yasuhiro Hatsugai, “Mirror skin effect and its electric circuit simulation,” *Phys. Rev. Res.* **2**, 022062 (2020).
- [21] Nobuyuki Okuma and Masatoshi Sato, “Hermitian zero modes protected by non-normality: Application of pseudospectra,” *Phys. Rev. B* **102**, 014203 (2020).
- [22] A. Ghatak, M. Brandenbourger, J. van Wezel, and C. Coulais, “Observation of non-hermitian topology and its bulk-edge correspondence in an active mechanical metamaterial,” *Proc. Natl. Acad. Sci. U.S.A.* **117**, 29561 (2020).
- [23] S. Weidemann, M. Kremer, T. Helbig, T. Hofmann, A. Stegmaier, M. Greiter, R. Thomale, and A. Szameit, “Topological funneling of light,” *Science* **368**, 311 (2020).
- [24] T. Helbig, T. Hofmann, S. Imhof, M. Abdelghany, T. Kiessling, L. W. Molenkamp, C. H. Lee, A. Szameit, M. Greiter, and R. Thomale, “Generalized bulk-boundary correspondence in non-hermitian topoelectrical circuits,” *Nat. Phys.* **16**, 747 (2020).
- [25] Tobias Hofmann, Tobias Helbig, Frank Schindler, Nora Salgo, Marta Brzezińska, Martin Greiter, Tobias Kiessling, David Wolf, Achim Vollhardt, Anton Kabaši, Ching Hua Lee, Ante Bilušić, Ronny Thomale, and Titus Neupert, “Reciprocal skin effect and its realization in a topoelectrical circuit,” *Phys. Rev. Res.* **2**, 023265 (2020).
- [26] L. Xiao, T. Deng, K. Wang, G. Zhu, Z. Wang, W. Yi, and P. Xue, “Non-hermitian bulk-boundary correspondence in quantum dynamics,” *Nat. Phys.* **16**, 761 (2020).
- [27] Wei Gou, Tao Chen, Dizhou Xie, Teng Xiao, Tian-Shu Deng, Bryce Gadway, Wei Yi, and Bo Yan, “Tunable nonreciprocal quantum transport through a dissipative aharonov-bohm ring in ultracold atoms,” *Phys. Rev. Lett.* **124**, 070402 (2020).
- [28] Nobuyuki Okuma and Masatoshi Sato, “Quantum anomaly, non-hermitian skin effects, and entanglement entropy in open systems,” *Phys. Rev. B* **103**, 085428 (2021).
- [29] Kohei Kawabata, Ken Shiozaki, and Shinsei Ryu, “Topological field theory of non-hermitian systems,” *Phys. Rev. Lett.* **126**, 216405 (2021).
- [30] Ryo Okugawa, Ryo Takahashi, and Kouta Yokomizo, “Non-hermitian band topology with generalized inversion symmetry,” *Phys. Rev. B* **103**, 205205 (2021).
- [31] Shuo Liu, Ruiwen Shao, Shaojie Ma, Lei Zhang, Oubo You, Haotian Wu, Yuan Jiang Xiang, Tie Jun Cui, and Shuang Zhang, “Non-hermitian skin effect in a non-hermitian electrical circuit,” *Research* **2021** (2021), 10.34133/2021/5608038.
- [32] X. Zhang, Y. Tian, J.-H. Jiang, M.-H. Lu, and Y.-F. Chen, “Observation of higher-order non-hermitian skin effect,” *Nat. Commun.* **12**, 5377 (2021).
- [33] L. S. Palacios, S. Tchoumakov, M. Guix, I. P. S. Sánchez, and A. G. Grushin, “Guided accumulation of active particles by topological design of a second-order skin effect,” *Nat. Commun.* **12**, 4691 (2021).
- [34] Dan Wu, Jia-Ming Xie, Yan-Qi Zhou, and Jun-Hong An, “Connections between the open-boundary spectrum and the generalized brillouin zone in non-hermitian systems,” *Phys. Rev. B* **105**, 045422 (2022).
- [35] Qian Liang, Dizhou Xie, Zhaoli Dong, Haowei Li, Hang Li, Bryce Gadway, Wei Yi, and Bo Yan, “Dynamic signatures of non-hermitian skin effect and topology in ultracold atoms,” *Phys. Rev. Lett.* **129**, 070401 (2022).
- [36] Fei Song, Hong-Yi Wang, and Zhong Wang, “Non-bloch pt symmetry: Universal threshold and dimensional surprise,” in *A Festschrift in Honor of the C N Yang Centenary* (WORLD SCIENTIFIC, 2022) pp. 299–311.
- [37] Stefano Longhi, “Non-hermitian skin effect and self-acceleration,” *Phys. Rev. B* **105**, 245143 (2022).
- [38] Zhen Gu, Hongyi Gao, Hong-Ye Xue, Jing Li, Zhi Su, and Jian Zhu, “Transient non-hermitian skin effect,” *Nat. Commun.* **13**, 7668 (2022).
- [39] Kohei Kawabata, Tokiro Numasawa, and Shinsei Ryu, “Entanglement phase transition induced by the non-hermitian skin effect,” *Phys. Rev. X* **13**, 021007 (2023).
- [40] Cun-An Li, Björn Trauzettel, Titus Neupert, and Shou-Cheng Zhang, “Enhancement of second-order non-hermitian skin effect by magnetic fields,” *Phys. Rev. Lett.* **131**, 116601 (2023).
- [41] Yi-Ling Zhang, Li-Wei Wang, Yang Liu, Zhao-Xian Chen, and Jian-Hua Jiang, “Hybrid skin-topological effect in non-hermitian checkerboard lattices with large chern numbers,” (2024), arXiv:2411.07465.
- [42] Daichi Nakamura, Takumi Bessho, and Masatoshi Sato, “Bulk-boundary correspondence in point-gap topological phases,” *Phys. Rev. Lett.* **132**, 136401 (2024).

- [43] Yusuke O. Nakai, Nobuyuki Okuma, Daichi Nakamura, Kenji Shimomura, and Masatoshi Sato, “Topological enhancement of nonnormality in non-hermitian skin effects,” *Phys. Rev. B* **109**, 144203 (2024).
- [44] Sho Ishikawa and Tsuneya Yoshida, “Non-hermitian F_4 skin effect protected by glide symmetry,” *Phys. Rev. B* **110**, 115301 (2024).
- [45] Xiao Zhang, Boxue Zhang, Weihong Zhao, and Ching Hua Lee, “Observation of non-local impedance response in a passive electrical circuit,” *SciPost Phys.* **16**, 002 (2024).
- [46] Zheng Wei, Ji-Yao Fan, Kui Cao, Xin-Ran Ma, and Su-Peng Kou, “Generalized non-hermitian skin effect,” (2025), [arXiv:2505.10252](https://arxiv.org/abs/2505.10252).
- [47] Ruizhe Shen, Tianqi Chen, Bo Yang, and Ching Hua Lee, “Observation of the non-hermitian skin effect and fermi skin on a digital quantum computer,” *Nature Communications* **16**, 1340 (2025).
- [48] Kohei Kawabata, Nobuyuki Okuma, and Masatoshi Sato, “Non-bloch band theory of non-hermitian hamiltonians in the symplectic class,” *Phys. Rev. B.* **101**, 195147 (2020).
- [49] Haiping Hu and Erhai Zhao, “Knots and non-hermitian bloch bands,” *Phys. Rev. Lett.* **126**, 010401 (2021).
- [50] Kouta Yokomizo and Shuichi Murakami, “Non-bloch band theory in bosonic bogoliubov-de gennes systems,” *Phys. Rev. B.* **103**, 165123 (2021).
- [51] Tianyu Li, Jia-Zheng Sun, Yong-Sheng Zhang, and Wei Yi, “Non-bloch quench dynamics,” *Phys. Rev. Res.* **3**, 023022 (2021).
- [52] Gang-Feng Guo, Xi-Xi Bao, and Lei Tan, “Non-hermitian bulk-boundary correspondence and singular behaviors of generalized brillouin zone,” *New Journal of Physics* **23**, 123007 (2021).
- [53] Wen-Tan Xue, Ming-Rui Li, Yu-Min Hu, Fei Song, and Zhong Wang, “Simple formulas of directional amplification from non-bloch band theory,” *Phys. Rev. B* **103**, L241408 (2021).
- [54] Kouta Yokomizo and Shuichi Murakami, “Scaling rule for the critical non-hermitian skin effect,” *Phys. Rev. B.* **104**, 165117 (2021).
- [55] Yang Li, Xiang Ji, Yuanping Chen, Xiaohong Yan, and Xiaosen Yang, “Topological energy braiding of non-bloch bands,” *Phys. Rev. B* **106**, 195425 (2022).
- [56] Haoshu Li and Shaolong Wan, “Exact formulas of the end-to-end green’s functions in non-hermitian systems,” *Phys. Rev. B* **105**, 045122 (2022).
- [57] Hongfang Liu, Ming Lu, Zhi-Qiang Zhang, and Hua Jiang, “Modified generalized brillouin zone theory with on-site disorder,” *Phys. Rev. B* **107**, 144204 (2023).
- [58] Tommy Tai and Ching Hua Lee, “Zoology of non-hermitian spectra and their graph topology,” *Phys. Rev. B* **107**, L220301 (2023).
- [59] Yu-Min Hu and Zhong Wang, “Green’s functions of multiband non-hermitian systems,” *Phys. Rev. Res.* **5**, 043073 (2023).
- [60] Yu-Min Hu, Yin-Quan Huang, Wen-Tan Xue, and Zhong Wang, “Non-bloch band theory for non-hermitian continuum systems,” *Phys. Rev. B* **110**, 205429 (2024).
- [61] Kota Matsushima and Takahiro Yamada, “Non-bloch band theory for time-modulated discrete mechanical systems,” (2024), [arXiv:2407.09871](https://arxiv.org/abs/2407.09871).
- [62] He-Ran Wang, Zijian Wang, and Zhong Wang, “Non-bloch self-energy of dissipative interacting fermions,” (2024), [arXiv:2411.13661](https://arxiv.org/abs/2411.13661).
- [63] K. Roy, K. Gogoi, and S. Basu, “Topological characterization of a non-hermitian ladder via floquet non-bloch theory,” (2024), [arXiv:2410.05427](https://arxiv.org/abs/2410.05427).
- [64] Zhenghao Yang, Chaoze Lu, and Xiancong Lu, “Entanglement entropy on generalized brillouin zone,” *Phys. Rev. B* **110**, 235127 (2024).
- [65] Yongxu Fu and Yi Zhang, “Braiding topology of non-hermitian open-boundary bands,” *Phys. Rev. B* **110**, L121401 (2024).
- [66] Shu-Xuan Wang and Zhongbo Yan, “General theory for infernal points in non-hermitian systems,” *Phys. Rev. B* **110**, L201104 (2024).
- [67] Sumit Verma and Min Jae Park, “Non-bloch band theory of sub-symmetry-protected topological phases,” (2024), [arXiv:2405.06240](https://arxiv.org/abs/2405.06240).
- [68] Yu-Min Hu, Hong-Yi Wang, Zhong Wang, and Fei Song, “Geometric origin of non-bloch \mathcal{PT} symmetry breaking,” *Phys. Rev. Lett.* **132**, 050402 (2024).
- [69] Q. Li, H. Jiang, and C. H. Lee, “Phase-space generalized brillouin zone for spatially inhomogeneous non-hermitian systems,” (2025), [arXiv:2501.09785](https://arxiv.org/abs/2501.09785).
- [70] Jia-Xin Zhong, Jing Lin, Kai Chen, Jing Lu, Kun Ding, and Yun Jing, “Unveiling non-hermitian band structures with non-bloch supercells,” (2025), [arXiv:2510.20160](https://arxiv.org/abs/2510.20160).
- [71] Haiyu Meng, Yee Sin Ang, and Ching Hua Lee, “Generalized brillouin zone fragmentation,” (2025), [arXiv:2508.13275](https://arxiv.org/abs/2508.13275).
- [72] Koustav Roy, Dipendu Halder, Koustabh Gogoi, B. Tanatar, and Saurabh Basu, “Floquet non-bloch formalism for a non-hermitian ladder: From theoretical framework to topoelectrical circuits,” (2025), [arXiv:2507.23744](https://arxiv.org/abs/2507.23744).
- [73] Daichi Nakamura, Yutaro Tanaka, Ken Shiozaki, and Kohei Kawabata, “Nonsymmorphic topological phases of non-hermitian systems,” (2025), [arXiv:2504.20743](https://arxiv.org/abs/2504.20743).
- [74] Shunyu Yao and Zhong Wang, “Edge states and topological invariants of non-hermitian systems,” *Phys. Rev. Lett.* **121**, 086803 (2018).
- [75] Tao Liu, Yu-Ran Zhang, Qing Ai, Zongping Gong, Kohei Kawabata, Masahito Ueda, and Franco Nori, “Second-order topological phases in non-hermitian systems,” *Phys. Rev. Lett.* **122**, 076801 (2019).
- [76] Kazuki Yokomizo and Shuichi Murakami, “Non-bloch bands in two-dimensional non-hermitian systems,” *Phys. Rev. B* **107**, 195112 (2023).
- [77] Hui Jiang and Ching Hua Lee, “Dimensional transmutation from non-hermiticity,” *Phys. Rev. Lett.* **131**, 076401 (2023).
- [78] Zeqi Xu, Bo Pang, Kai Zhang, and Zhesen Yang, “Two-dimensional asymptotic generalized brillouin zone theory,” (2023), [arXiv:2311.16868](https://arxiv.org/abs/2311.16868).
- [79] Kun Zhang, Zhesen Yang, and Kai Sun, “Edge theory of non-hermitian skin modes in higher dimensions,” *Phys. Rev. B.* **109**, 165127 (2024).
- [80] Kai Zhang, Chang Shu, and Kai Sun, “Algebraic non-hermitian skin effect and generalized fermi surface formula in arbitrary dimensions,” *Phys. Rev. X* **15**, 031039 (2025).
- [81] Chenyang Wang, Jinghui Pi, Qinxin Liu, Yaohua Li, and Yong-Chun Liu, “Universal theory for geometry-dependent non-hermitian bands,” (2025), [arXiv:2506.22743](https://arxiv.org/abs/2506.22743).
- [82] Ayan Banerjee, Rimika Jaiswal, Madhusudan Manju-

- nath, and Awadhesh Narayan, “A tropical geometric approach to exceptional points,” *Proceedings of the National Academy of Sciences* **120**, e2302572120 (2023).
- [83] Hong-Yi Wang, Fei Song, and Zhong Wang, “Amoeba formulation of non-bloch band theory in arbitrary dimensions,” *Phys. Rev. X* **14**, 021011 (2024).
- [84] Shu-Xuan Wang, “Constraints of internal symmetry on the non-hermitian skin effect and bidirectional skin effect under the action of the hermitian conjugate of time-reversal symmetry,” *Phys. Rev. B* **109**, L081108 (2024).
- [85] Yuncheng Xiong and Haiping Hu, “Graph morphology of non-hermitian bands,” *Phys. Rev. B* **109**, L100301 (2024).
- [86] Yuncheng Xiong, Ze-Yu Xing, and Haiping Hu, “Non-hermitian skin effect in arbitrary dimensions: non-bloch band theory and classification,” (2024), [arXiv:2407.01296](https://arxiv.org/abs/2407.01296).
- [87] Haiping Hu, “Topological origin of non-hermitian skin effect in higher dimensions and uniform spectra,” *Science Bulletin* **70**, 51–57 (2025).
- [88] G Szegő, “Ein grenzwertsatz über die toeplitzischen determinanten einer reellen positiven funktion,” *Math. Ann.* **76**, 490–503 (1915).
- [89] Harold Widom, “Asymptotic behavior of block toeplitz matrices and determinants,” *Advances in Mathematics* **13**, 284–322 (1974).
- [90] Harold Widom, “Asymptotic behavior of block toeplitz matrices and determinants. ii,” *Advances in Mathematics* **21**, 1–29 (1976).
- [91] Shin Kaneshiro and Robert Peters, “Symplectic-amoeba formulation of the non-bloch band theory for one-dimensional two-band systems,” *Phys. Rev. B* **112**, 075408 (2025).
- [92] Abhijeet Alase, Emilio Cobanera, Gerardo Ortiz, and Lorenza Viola, “Wiener–hopf factorization approach to a bulk-boundary correspondence and stability conditions for topological zero-energy modes,” *Annals of Physics* **458**, 169457 (2023).
- [93] E. Basor, J. Dubail, T. Emig, and R. Santachiara, “Modified szegő–widom asymptotics for block toeplitz matrices with zero modes,” *Journal of Statistical Physics* **174**, 28–39 (2019).